Journal of Materials Science: Materials in Electronics (2019) 30:9065–9086
https://doi.org/10.1007/s10854-019-01333-w

REVIEW

The reliability of lead-free solder joint subjected to special environment: a review

Jianhao Wang[1] · Songbai Xue[1] · Peng Zhang[1] · Peizhuo Zhai[1] · Yu Tao[1]

Received: 22 January 2019 / Accepted: 12 April 2019 / Published online: 19 April 2019
© Springer Science+Business Media, LLC, part of Springer Nature 2019

Abstract

With the rapid development of electronical products, many primary challenges arise in the field of design and manufacture, among which the property of electronical packaging materials is a crucial factor. Compared with lead-containing solder, the performance of lead-free solder alloy is hardly noticed before but is being concerned recently due to the restriction of lead application, which still could not meet the actual requirement. Moreover, the increasingly severe service conditions of electronical equipment such as specific temperature, high-density current and corrosion, which would result in the degradation of microstructure and property of lead-free solder alloy, have requested a great raise in the reliability of solder joint. Therefore, a great number of studies to enhance the reliability of lead-free solder joint subjected to special environments have been conducted in the last decade and it has been proved that the increasing reliability could be obtained by the addition of element and nanoparticle, as well as the enhanced substrate. In this article, a systematic review of the progress on the reliability investigation of lead-free solder joint is given to try to provide some theoretical support for the further investigation and application of lead-free solder alloy.

1 Introduction

Traditional Pb-containing solder alloy has been widely applied in the last century due to its excellent property and low cost. But with the implement of the directives on waste electrical and electronic equipment (WEEE) and restriction of the use of hazardous substances in electrical and electronic equipment (RoHS Directive), much requirement has been attached to lead-free solder alloys, the majority of which are SnCu, SnZn, SnBi and SnAgCu systems [1]. However, compared to lead-containing solder alloy, the effect of thermal/electrical stress and corrosive mediums on lead-free solders is more severe and consequently, the unsatisfactory reliability of lead-free solder alloys has been limited their application.

With the advance of technology, the miniaturization and high power have become the essential factor of electronic devices which benefit from the application of high-density integrated circuit packages, such as BGA, CSP, IGBT and WLP. The decreasing size of packaging has placed much importance on the reliability of solder alloy, especially under the drive of increasingly severe service environment of electronic device. Miniature solder joints are being subjected to specific temperature, high-density current and corrosive environment, which would significantly degrade the property of solder joint and even result in the fracture of electronic system [2–5]. Therefore, it is worthy of attention to understand the failure mechanism of lead-free solder joints under special environments and seek the solution to improve their reliability. In this paper, the reliability evolution of three typical lead-free solder joints under various special environments was summarized, including isothermal aging, thermal cycling, cryogenic storage, electromigration, corrosion and radiation. Moreover, the investigation progress on enhancing the reliability of lead-free solder joint was discussed, expecting to provide some suggestions for the further reliability research of lead-free solder alloy.

2 Isothermal aging

2.1 Influence mechanism

2.1.1 SnAgCu solder alloy

The microstructure of SnAgCu solder matrix is mainly comprised of β-Sn dendrites, along with small Cu_6Sn_5 and

✉ Songbai Xue
xuesb@nuaa.edu.cn

[1] College of Materials Science and Technology, Nanjing University of Aeronautics and Astronautics, Nanjing 210016, China

Ag_3Sn particles [6]. These particles dispersed in the matrix, enhancing the microstructure of solder joint and however, they coarsened during thermal aging because of the accelerated atomic migration, which broke the dendritic structure and resulted in the formation of voids in the solder matrix [7]. It is well known that the reliability of solder joint is influenced by the thickness and morphology of brittle intermetallic compound (IMC) layer between solders and Cu substrate, such as Cu_6Sn_5, Cu_3Sn, etc. Due to increasing service temperature, the excessive growth of Cu_6Sn_5 layer and the formation of new Cu_3Sn layer could be obtained, which gave a decrease in the reliability of solder joints [8]. As could be observed in Fig. 1, Cu_6Sn_5 layer of SnAgCu solder joint significantly thickened after isothermal aging and a new Cu_3Sn layer formed between Cu_6Sn_5 and Cu substrate with a few voids due to the atomic migration [9]. The competitive growth of two brittle IMC layer increased the initiation risk of crack in solder joint, hence the mechanical property of joint was degraded [10].

2.1.2 SnBi solder alloy

As a typical eutectic structure, SnBi solder matrix consists of lamellar β-Sn and Bi phase, which interlock with each other [11]. The diffusion rate between Sn/Bi phase was risen during thermal aging and the increasing eutectic space of SnBi solder matrix was observed. As the brittleness of Bi was significantly higher than other chemical compositions, the mechanical property of SnBi solder joint was decreased due to the coarsening Bi phase near the interface, as well as the excessive growth of Cu_6Sn_5 and Cu_3Sn layer [12, 13]. Zou et al. [14] investigated the aging effect on the SnBi/Cu solder joint and found the solder joint almost failed after aged at 120 °C for only 324 h. Although SnBi is a promising low-melting temperature filler metal, it has been proved that Bi element could accelerate the growth of brittle IMC layer of Sn-based solder joint [15]. Therefore, the reliability of SnBi solder joint subjected to thermal stress should be greatly concerned.

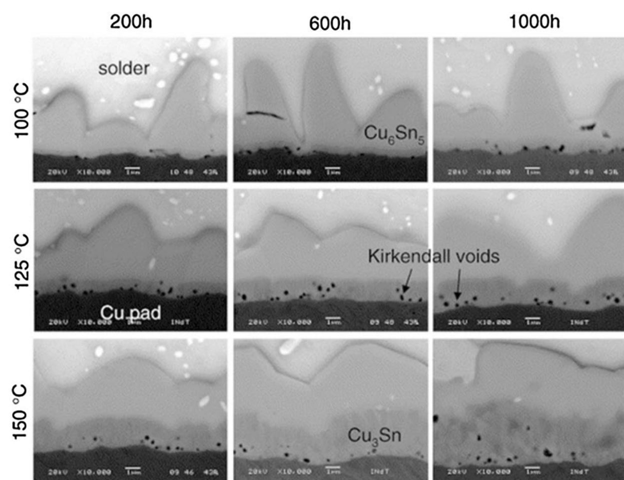

Fig. 1 Evolution of interfacial structure at various aging temperature and time [9]

2.1.3 SnZn solder alloy

SnZn solder alloy is seen as an excellent candidate for Pb-containing solder because of its melting temperature and cost, but its reliability is always a non-negligible problem. The β-Sn and needle-like Zn-rich phase form the microstructure of SnZn matrix [16]. Owing to the high chemical activity of Zn, the growth of Zn-rich phase during aging process is harmful to the reliability of solder joint, especially for these exposed to thermal and corrosive conditions [17]. Unlike other Sn-based solder alloy, the interfacial layer of SnZn solder joint is Cu_5Zn_8 intermetallics rather than Cu-Sn and the accelerated growth of Cu_5Zn_8 layer at high-temperature storage is also a great reason for the reducing reliability [18]. Xue et al. [19] found that after aged at 150 °C for 1200 h, the Cu_5Zn_8 layer of SnZnGa solder joint significantly thickened with a shear strength decrement of approximately 49.33%.

2.2 Micro-alloying

2.2.1 Rare earth elements

Rare earth(RE) elements are seen as the excellent modifier for electronic packaging materials [20]. The trace addition of Nd could significantly improve the microstructure stability of SnAgCu solder joints at the elevated temperature, which could be attributed to the grain refinement strengthening of dispersed Nd-Sn particles [21]. Moreover, it was reported that compared with SnAgCu solder, finer Ag_3Sn particles would aggregate at the interface of SnAgCu-Ce solder joint, which decreased the thickness and grain size of the IMC layer and reduced the fracture risk, as shown in Fig. 2 [22]. The effect of Ce and La mixed RE addition on SnBi solder joint was quite similar and in the comparison with SnBi, the IMC layer of SnBi-0.1RE was hardly changed during thermal aging because RE could depress the activity of Sn, giving a lower growth rate of IMC [23]. After aged at different temperature for up to 1200 h, SnZnGa-Nd solder performed better than SnZnGa and SnZn solder joints in the strength test, which was attributed to the more stable microstructure of SnZnGa-Nd solder [24]. But after the content of rare earth elements exceeded a critical value, coarsening RE phase formed in the solder matrix and hence the reliability degradation of solder joints was obtained [25].

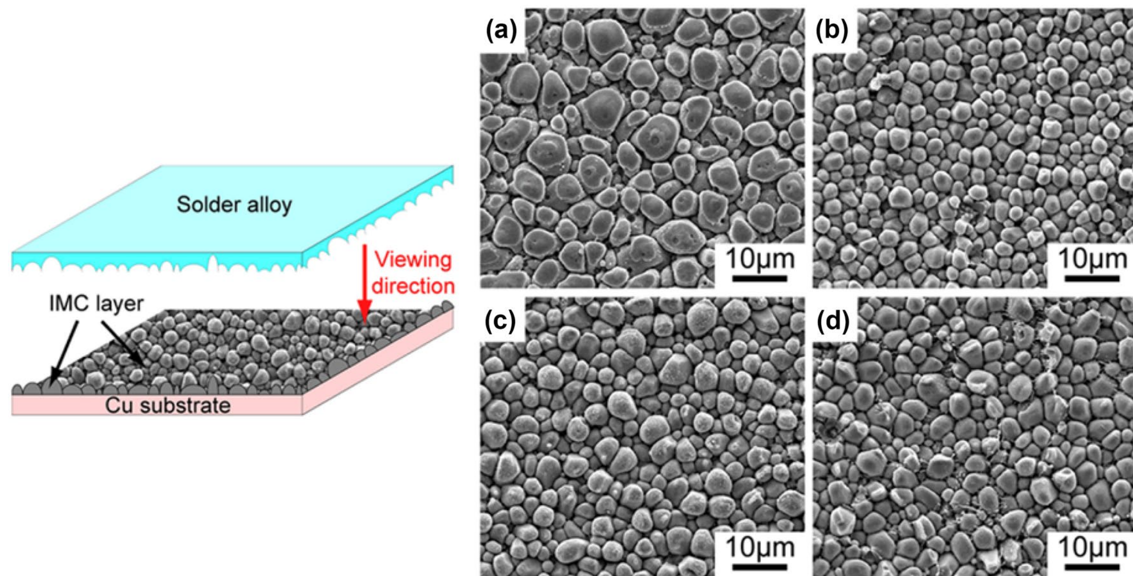

Fig. 2 Top-view morphology of the Cu_6Sn_5 particles between the solder alloys and the Cu substrate in as-reflowed conditions for the alloy **a** SnAgCu; **b** SnAgCu-0.02Ce; **c** SnAgCu-0.15Ce; **d** SnAgCu-0.5Ce [22]

2.2.2 Other metallic elements

Previous researches showed that doping Mn reduced the space between Cu_6Sn_5 particle and the diffusion of Sn across interface of SnAgCu-Mn solder joint became more difficult [26, 27]. Hence after 200 h aging, only Cu_6Sn_5 layer was observed whose thickness was thinner than SnAgCu solder joint. The thickness of IMC layer during thermal aging could be expressed as follows:

$$Y = Y_0 + \sqrt{Dt} \tag{1}$$

where Y_0 is the IMC thickness of as-soldered joint and D is the diffusion coefficient of atoms that is positive correlated with temperature. The addition of Ge could impede the diffusion of Cu into solder matrix and as listed in Table 1, although the diffusion coefficient was increased with rising temperature, the coefficient of SnCu-Ge solder joint was lower than SnCu, which inhibited the excessive growth of IMC layer [28]. Compared with SnAgCu solder, the thermal fatigue resistance of the SnAgCu solder joint modified with Bi was significantly improved due to the strengthening effect of solid-soluted Bi in Sn matrix and it had been proved that the microstructure of SnAgCu solder doping with Bi and Fe remained more stable during thermal aging, which might be concluded that multi-additions could be an excellent method to improve the reliability of lead-free solder [29, 30]. Zhang et al. [31] reported that a Cu-Ag layer formed at the interface of SnBi-Ag/Cu solder joint, which depressed the growth of IMC layer as well as Bi segregation during the soldering and aging process. This was ascribed to the impeding effect of Cu-Ag layer and Ag_3Sn particle on the atomic diffusion. Ni was claimed to be conducive to refining the microstructure of SnBi solder and postponing the coarsening behavior of Bi-rich phase by the formation of concentrated Ni_3Sn_4 on solder matrix [32]. Hu et al. [18] investigated the effect of Cr addition on SnZn solder and found that lower diffusion coefficient and constant of Cu_5Zn_8 was obtained in SnZn-0.3Cr solder because Cr could reduce the activity of Zn by generating Zn-Cr phase.

Table 1 Diffusion coefficient at different temperatures [28]

Temperature (°C)	Diffusion coefficient, D ($\mu m^2/h$)	
	SnCu	SnCu-Ge
100	0.001421	0.001163
125	0.013433	0.005898
150	0.066409	0.028696

2.3 Nanoparticle strengthening

2.3.1 Metallic nanoparticles

Thanks to the nano-size effect, the property of metal materials could be greatly influenced by the addition of nanoparticles and solder alloys are no exception. As illustrated in Fig. 3, although thermal aging reduced the ultimate tensile strength of solder joint, the strength improvement of SnAgCu solder joint bearing nano-Mn was attained at the same isothermal aging parameter due to the strengthening effect of nano-Mn pinning at the grain boundary, peaking at

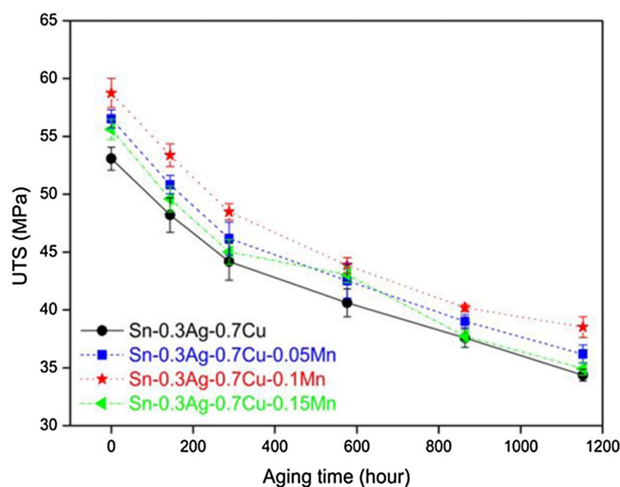

Fig. 3 UTS versus aging time of Sn–0.3Ag–0.7Cu–xMn solder joints aged at 150 °C [33]

0.1 wt% nano-Mn [33]. However, it has been proved that the content of nano-Mn should be limited to less than 0.15 wt% and otherwise Mn nanoparticle would reunite to form large particles and the coarsening microstructure was observed again [34]. Ag_3Sn nanoparticles tended to assemble at the interface of solder joints and blocked the migration of IMC grain boundary, which refined the microstructure and enhanced the properties [35].

2.3.2 Compound nanoparticles

With the identical element content, the reliability of SnAg solder doping with Ag_3Sn nanoparticle was better than that of SnAgCu solders [36]. Meanwhile, the stress magnitude of SnAgCu-TiO_2 solder joint was reduced with the decrease of the pad size during the thermal aging, which minimized the probability of the formation of crystal defects and improved joint reliability [37]. Sharma et al. [38] added 0.6 wt% nano-CeO_2 into SnBi solder alloy and found that the strength of joint was remarkably enhanced with a symmetrical microstructure. During the long-term aging, the IMC layer growth of SnBi-nanoCeO_2 solder joint was more unobvious than SnBi, providing an excellent reliability. A similar phenomenon was observed in the SnZnBi solder bearing ZrO_2 nanoparticle where Zn atoms was impeded from gathering due to the blocking effect of nano ZrO_2 [39]. Consequently, the excessive growth of Cu_5Zn_8 layer during isothermal aging was restrained.

2.3.3 Advanced nanoparticles

Doping Graphene nanosheets (GNSs) not only improved the wettability of lead-free solders by reducing the interfacial surface energy between solder and substrate [40], but also significantly impeded the diffusion across the interface, which depressed the excessive growth of IMC layer and increased the mechanical properties of solder joints, as shown in Fig. 4 [41, 42]. Carbon nanotube (CNT) is another type of excellent strengthening phase for lead-frees solder alloys. Yang et al. [43] found that Ni-CNTs could reduce the thermal expansion coefficient (CTE) of SnBi solder and hence gave a thinner IMC layer than original solder during thermal aging.

Despite the enhanced reliability of lead-free solder joint was obtained by modifying nanoparticles, nanoparticles possessed few effect on melting characterization of solder alloy compared with micro-alloying. Meanwhile, the manufacture of lead-free solder bearing nanoparticles is usually expensive, which limits their application.

2.4 Enhanced substrate

Considering that the coarsening IMC layer induced by the diffusion becomes the weak area of solder joint after thermal aging, strengthening substrate to postpone the growth of IMC layer is seen as an excellent method to improve the reliability of lead-free solder with superior operability [44, 45]. Recently great attractions have been placed on the surface finish technology of Cu pad, impeding the diffusion of Cu in solder matrix. So far various coatings have been applied,

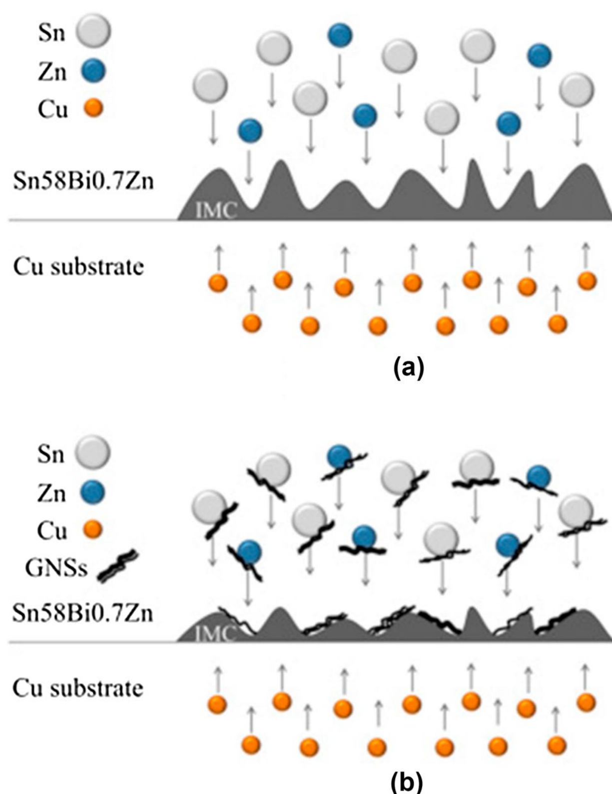

Fig. 4 Schematic diagram of the IMC growth at the **a** undoped and **b** GNS-doped Sn58Bi0.7Zn solder joint interface [42]

the majority of which are Ni, electroless nickel-immersion gold (ENIG), electroless nickel electroless palladium immersion gold (ENEPIG) and organic solderability preservative (OSP). In SnAg/Ni-Cu solder joint, the diffusion of Cu in solder matrix during thermal aging could be impeded by the Ni surface finish which acted as a barrier layer, and a new Ni_3Sn_4 IMC layer formed, whose growth rate was lower than Cu_6Sn_5 and Cu_3Sn [46]. Although Cu pad with Ni film performed well in the test, the solderability of lead-free solder alloy would be declined due to the oxidation of Ni film during the thermal storage. Therefore, Au was sprayed on the Ni surface to prevent it from being exposed to air and enhance the wettability of the molten solder, which was known as ENIG [47]. Compared with ENIG, currently ENEPIG surface coating is applied much more widely because Pd layer in ENEPIG could suppress the growth of interfacial layer and the consumption of Ni layer, strengthening thermal stability of solder joint [48]. Therefore, as illustrated in Fig. 5, the enhancement effect of ENEPIG was more notable than ENIG and OSP, with higher microstructure stability of solder joint during aging [49]. But it has been proved that the thickness of Pd layer should be limited below 0.2 µm or the formation of $(Ni, Cu)_3Sn_4/Ni_2Sn$ bilayer with a series of micro-cracks would be attained, which was induced by the poor attachment of two layers [50].

Besides surface films, alloying Cu substrate is also able to improve the reliability of lead-free solder joint, which is an emerging investigation for now. Zhang et al. [51] modified Cu pad by doping minor amount of Ag and Zn and the results showed that the addition of Ag and Zn could restrain the Bi segregation at the interface of SnBi/Cu-X solder joint after thermal aging and therefore the Bi embrittlement was eliminated, as shown in Fig. 6. Moreover, during aging, the formation of Cu_3Sn and Kirkendall voids was significantly hindered in the SnAgCu/Cu-2Mn solder joint, which could be attributed to the Mn segregation in Cu_3Sn layer [52].

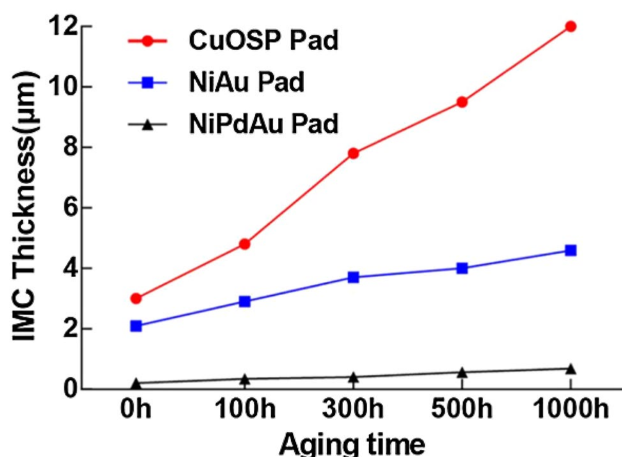

Fig. 5 The IMC thickness of SnAgCu solder joint with different surface films after aging at 150 °C [49]

Cu_3Sn layer doping Mn acted as a diffusion barrier for solder/Cu interface and resulted in the slower growth rate of interfacial layer. Compared with surface coating, alloying Cu substrate with the character of more easily operating and lower cost, could be a novel idea to enhance the reliability of lead-free solder joint.

3 Thermal cycling

3.1 Influence mechanism

3.1.1 SnAgCu solder alloy

The changing power of electrical production provides a periodic temperature cycle in the electronical devices, which could affect the property of solder joint. During the high-temperature stage, the growing IMC layer of SnAgCu was observed with the formation of Cu_6Sn_5/Cu_3Sn bilayer microstructure, which was similar to thermal aging [53]. Exposed to the low-temperature condition, the stress at the interface would greatly improve due to the different CTE of brittle Cu_3Sn and Cu_6Sn_5 and hence micro-defects were generated [54]. Hence after long-term cycling, the strength of solder joint was decreased with higher risk of failure [55]. Now a series of researches have been conducted to test the reliability of solder joint under thermal cycling conditions, the majority of which focus on the temperature range of − 65 to 150 °C [56, 57]. Recently, some investigations are starting to explore the reliability sensitivity of solder joint to the extreme thermal shocking due to the increasingly specific service environment. Tian et al. [58, 59] investigated the effect of − 196 °C/+ 150 °C thermal shocking on the reliability of SnAgCu/Cu solder joint and found significate deterioration was obtained with increasing shock cycles. The tensile strength of SnAgCu solder joint was reduced by 33% after only 300 cycles and big cavities formed in the solder matrix. Compared with the common thermal cycling test, more efforts should be put into the reliability investigation of solder joint subjected to extreme thermal shocking to meet the increasing requirement of electronical system.

3.1.2 SnBi solder alloy

In comparison with SnAg-based solders, SnBi solder seemed to suffer more greatly from thermal cycling at the same parameter [60]. Not only the excessive growth of brittle IMC layer, but also the coarsening Bi-rich phase along with big voids were observed after thermal cycling [61]. Cracks was generated in SnBi solder joint as well, which was attributed to the mismatch of CTE, and the coarsening brittle Bi-rich phase promoted its propagation process [62]. It may be concluded that as a low melting temperature

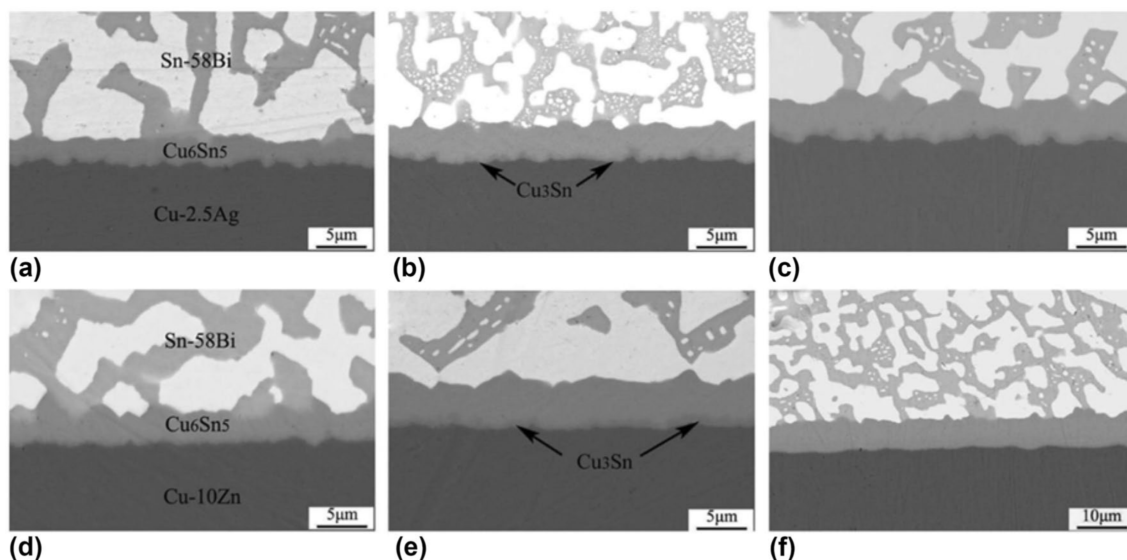

Fig. 6 Interfacial morphologies (backscattered electron image) of Sn–58Bi/Cu–2.5Ag solder joints aged for **a** 7 days, **b** 13 days, **c** 20 days, and Sn–58Bi/Cu–10Zn solder joints aged for **d** 7 days, **e** 13 days, and **f** 20 days [51]

solder alloy, the reliability deterioration of SnBi solder joint applied in the large-range temperature conditions should be seriously emphasized.

3.1.3 SnZn solder alloy

Bearing a resemblance to SnBi solder, SnZn solder joint also showed a microstructure degeneration after long-term thermal cycling. Increasing inner stress induced by thermal expansion, generated micro-cracks and CTE mismatch between β-Sn and Zn-rich phase during thermal cycling resulted in the faster crack growth [63, 64]. It was reported that the lifetime of SnZn solder joint under thermal cycling was also shorter than SnAgCu solder joint. Zhang et al. [65] estimated the reliability of Sn9Zn, Sn3.8Ag0.7Cu and Sn37Pb solder alloy through finite element analysis and found that due to lower von Mises stress, Sn9Zn showed longer fatigue life than Sn37Pb solder during thermal cycling test, which however failed to reach to the reliability level of Sn3.8Ag0.7Cu.

Currently the researches on the reliability of SnZn and SnBi solder subjected to thermal cycling are not sufficient enough but existing results indicate that SnAgCu solder performs better than other lead-free solder alloys during thermal cycling.

3.2 Micro-alloying

3.2.1 Rare earth elements

A series of investigations have proved that the addition of RE elements, such as Ce and Pr, could greatly improve the thermal cycling resistance of lead-free solder joints due to the RE-Sn particles in solder matrix, which refined β-Sn and acted as a barrier to the migration of grain boundary [66, 67]. Shen et al. [68] added a trace amount of La-Ce mixed RE in SnBiCu solder joint and found the similar phenomenon where finer Bi-rich phase and thinner IMC layer were observed, ensuring the excellent mechanical property of solder joint. It was reported that Y element not only contributed to improving the wettability of SnZn solder alloy, but also enhanced the strength of joint, which was always higher than SnZn solder joint at the same cycling parameter [69].

3.2.2 Other metallic elements

Wang et al. [70] investigated the effect of Bi addition on the microstructure and properties of SnAgCu solder. Results demonstrated that a moderate amount of Bi element led to the microstructural refinement and gave a significant increase of the strength because Bi element assembled at grain boundaries and offered a resistance to dislocation glide, especially with 3 wt % Bi addition. Compared with Sn–0.5Cu solder joint, the formation of (Al, Cu)-Sn, Si–Sn and Al–Sn particles was observed near the interface of Sn–0.5Cu modified with minor Al and Si, and the excessive IMC growth of Sn-0.5Cu solder joint during thermal cycling could be impeded by these particles [71]. But solder joints doping with composite additive of multiple elements do not always perform well. Although the composite addition of Ni, Sb and Bi could suppress the coarsening IMC layer of SnAgCu solder joint during the early stage of cycles, cracks expanded faster after certain cycles which was attributed

to the early recrystallization of Sn matrix [72]. It could be concluded from the result of electron back-scattered diffraction (EBSD) that the crack was easier to propagate in the recrystallization area due to the decreasing resistance of the massive grain boundaries which was generated at the early stage of thermal cycling, as shown in Fig. 7.

3.3 Nanoparticle strengthening

3.3.1 Metallic nanoparticles

Gain et al. [73] studied the reliability of SnAgCu-nano Al solder subjected to thermal cycling and found that the accumulation of Al nanoparticle on the grain boundary not only improved the mechanical properties of solder joints, but also reduced the diffusion coefficient of Cu across the interface during thermal cycling, which decreased the growth rate of brittle IMC layer. Mo nanoparticles, dispersing in SnBi-nano Mo solder matrix, were conducive to hindering the sliding of dislocation and make the mechanical property of composite solder joint enhanced [74].

3.3.2 Compound nanoparticles

Al_2O_3 nanoparticles, pinning at the grain boundaries of solder matrix, refined the β-Sn grain size and enlarged the content of eutectic microstructure in solder joint and therefore, gave an increasing strength of solder joint after thermal cycling. It could be seen from Fig. 8 that the shear force of 1 wt% nanoAl_2O_3-doped SnAgCu solder joint was still higher than original SnAgCu solder joint after 300 cycles, which was attributed to pinning effect of Al_2O_3 nanoparticles [75]. The total pinning force (F_{total}) of nanoparticles acting on the grain boundary of solder matrix could be expressed as follows:

$$F_{total} = n_i \pi r \gamma_b = \frac{3}{2}\frac{f\gamma_b}{r} \quad (2)$$

where n_i is the density of the nanoparticle at the grain boundary and r is the radius of the nanoparticle. It could be concluded that the F_{total} of nanoparticle acting on the grain boundary was positive correlated with the radius of particle and the effect of smaller nanoparticles on solder matrix was much more significant, resulting in finer microstructure and higher strength. As show in Fig. 9, TiO_2 nanoparticle with a diameter of 6 nm showed more notable effect on the SnAgCu solder matrix than those with a diameter of 20 nm [76]. Nano-Fe_2O_3 addition could remarkably improve the wettability of SnAgCu solders and reduce the CTE mismatch between the solder and substrate, which improved the reliability of solder joints under thermal cycling [77, 78].

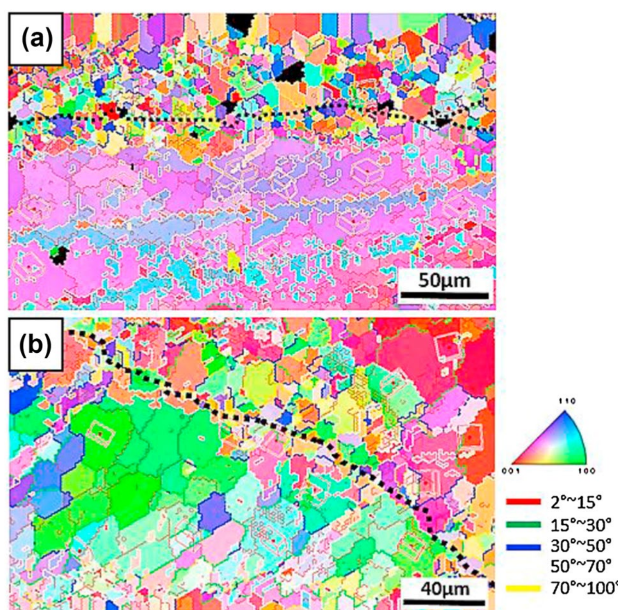

Fig. 7 The EBSD result of solder joint after 1500 thermal cycles: **a** SnAgCu, **b** SnAgCu-Ni-Sb-Bi [72]

3.3.3 Advanced nanoparticles

Ni-CNTs were claimed to be able to improve the microstructure stability of SnAgCu composite solder joint and after more than 2000 cycles, the joint still provided a reliable mechanical interconnection without obvious defects [79]. Polyhedral Oligomeric Silsesquioxane (POSS) nanoparticle with special structure, is seen as a novel reinforcing phase to the lead-free solder. Han et al. [80] found that 3 wt% POSS nanoparticle pinned the grain boundary of SnAgCu solder joints, resulting in the refined microstructure and the postponement of dislocation migration and crack initiation. What is more, POSS nanoparticles, accumulating at the interface of solder joint, acted as a barrier to the atomic diffusion between solder matrix and Cu substrate. As a result, the thinner brittle interfacial layer without crack initiation and the higher reliability of the solder joint were obtained, as shown in Fig. 10 [81].

3.4 Enhanced substrate

Compared with ENIG finishes, finer Ag_3Sn and Cu_6Sn_5 particles could be obtained in SnAgCu/OSP solder joint which had an enhancing effect on the strength of solder joint and obstructed the expansion of cracks induced by thermal cycling [82]. Therefore as shown in Fig. 11, SnAgCu/OSP-Cu solder joint performed better than SnAgCu/ENIG-Cu solder joint in the thermal cycling test [83]. Fe–Ni UBM provided an excellent barrier layer to the diffusion of Cu atoms during thermal cycling and hence the growth of the interfacial layer was slower than SnAgCu/Cu solder joint.

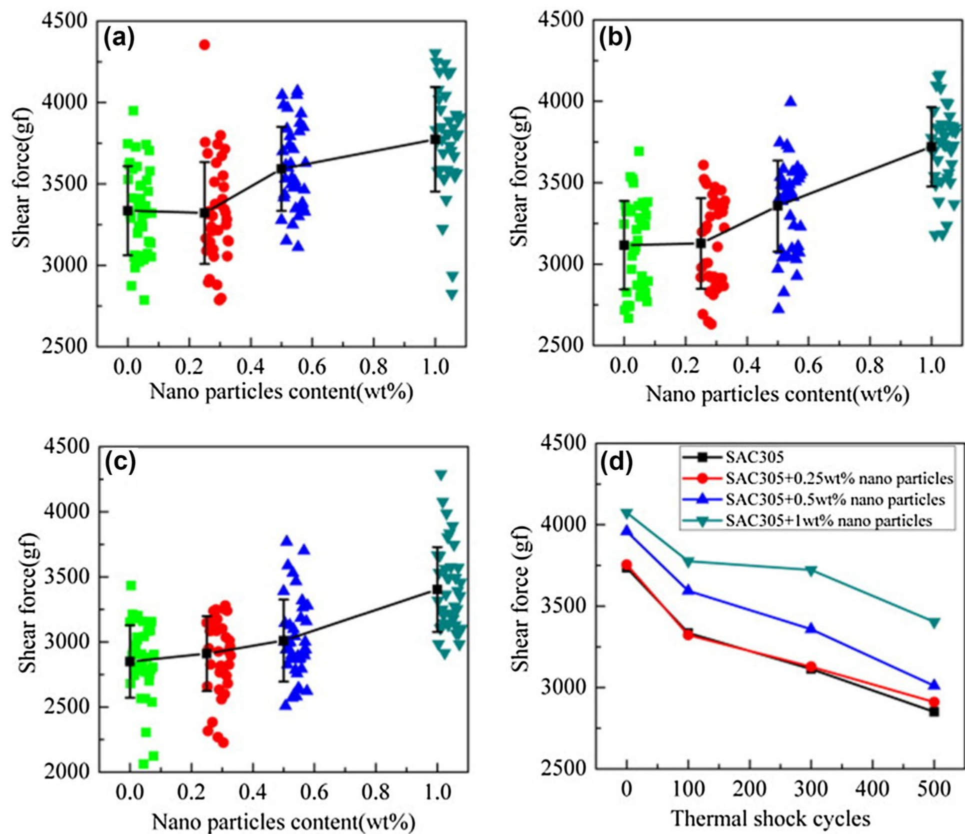

Fig. 8 Shear results comparison of SnAgCu-nanoAl_2O_3 solder joints after **a** 100, **b** 300, **c** 500 thermal shock cycles and **d** comparison of the average value [75]

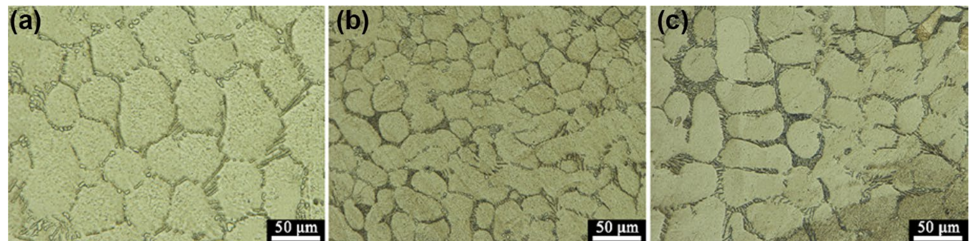

Fig. 9 Metallograph of the nano-composite solders (0.5 wt % TiO_2 nanoparticles): **a** SnAgCu; **b** SnAgCu-6 nm TiO_2; **c** SnAgCu-20 nm TiO_2 [76]

However the thermal stress in SnAgCu/Fe–Ni/Cu solder joint was increased due to CTE mismatch, which reduced the lifetime of solder joint [84]. Cai et al. [85] electroplated Co-P film on Cu substrate and found that small needle-shaped $CoSn_3$ and columnar $(Cu, Co)_6Sn_5$ IMC formed at the interface of SnAgCu/Co-4 wt%P solder joint and compared with SnAgCu/Cu solder joint, the higher strength after cycling was obtained due to the enhancing effect of small $CoSn_3$ particles. But for SnAgCu/Co-8 wt%P solder joint after thermal cycling, a brittle layer of Co-Sn-P was observed at the interface and hence the fracture occurred at the Co-Sn-P layer rather than solder matrix. Moreover, the fracture analysis showed that the type of fracture was changed from ductile to ductile–brittle mixed, as shown in Fig. 12.

Recently epoxy-contained lead-free solder paste attracts much attention. Although epoxy didn't change the chemical composition of solder matrix, it could form an insulation film over solder joints during soldering, which relieved residual stress and suppressed IMC growth, giving an enhanced reliability of joints [86, 87]. As illustrated in Fig. 13, the fracture of epoxy-containing SnAgCu solder joint was not observed after 1000 cycles and only a few pores formed in the solder matrix as well as epoxy. Moreover, insulating epoxy layer still attached well to solder joint during cycling, enhancing its mechanical property and stability [88].

4 Cryogenic storage

4.1 Influence mechanism

Generally, the service temperature of civil electronic products is no less than − 65 °C, which is also the lowest test temperature of production reliability. But the on-orbit

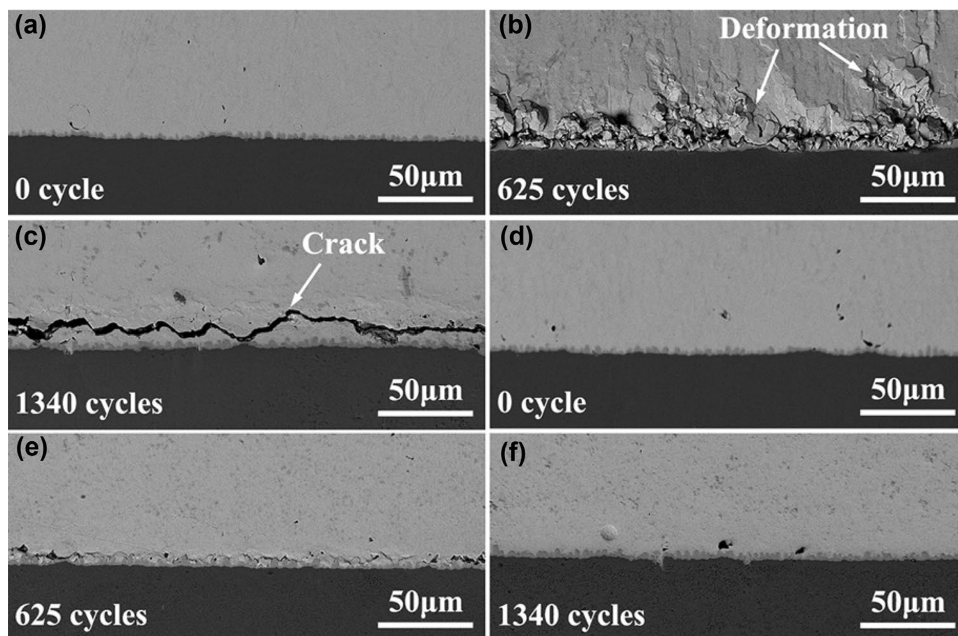

Fig. 10 Evolution of the microstructure at the interface during thermal cycling: **a**–**c** SnAgCu and **d**–**f** SnAgCu + 3 wt %POSS [81]

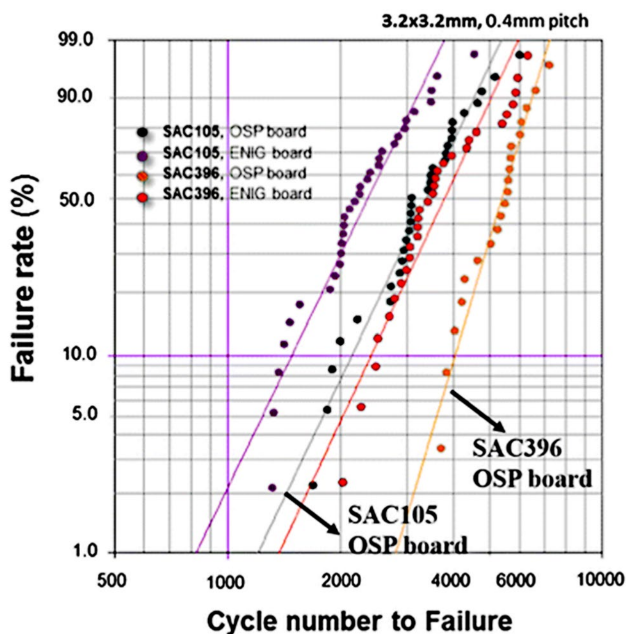

Fig. 11 Weibull plots of thermal cycling results for SnAgCu/OSP and SnAgCu/ENIG joints [83]

satellites travelling in deep space, such as the New Horizons and Juno of NASA, is subjected to the specific cryogenic environment, which is as low as near absolute zero of temperature. Currently the active thermal control system is applied to keep a suitable inner temperature, which however increases the volume and weight of satellite and fails to meet the miniaturization and light-weighting requirement of deep space exploration mission. As a result, the reliability of lead-free solders exposed to cryogenic condition becomes an important issue to provide the reference to reduce the active thermal control system of future small satellite.

As the majority of commercial solder is Sn-based alloy, the transition of β-Sn to α-Sn under cryogenic condition which is also called tin pest, is a serious problem to electronic devices, especially for lead-free solder alloy. NASA reported that eutectic SnPb solder alloy performed better than Sn–5Ag solder alloy in cryogenic strength test because Pb could impede the tin pest process. Lead-free solder joints subjected to cryogenic condition are in danger of fracture due to the difference of CTE and brittleness between β-Sn and α-Sn. As shown in Fig. 14, volume difference between α/β-Sn and the formation of crack could be observed after long-term cryogenic storage [89]. Tian et al. [90] studied the strength and fracture mechanisms of SnAgCu solder joints under specific cryogenic conditions and results showed that the tensile strength of SnAgCu solder joints was increased firstly and then decreased with descending temperature and the fracture mechanism changed from ductile mode to brittle mode because the CTE mismatch between solder and IMC layer became larger. With the aging temperature decreasing, the growth of Cu_6Sn_5 IMC layer was postponed while Ag_3Sn assembled at the interface and the degradation of ductility was obtained [91].

4.2 Improving measures

Although the application of lead has been forbidden, doping with other elements also help to increase the cryogen-resistance of solder alloy. It has been proved that the microstructure stability of Sn–0.5Cu solder doping with trace Bi

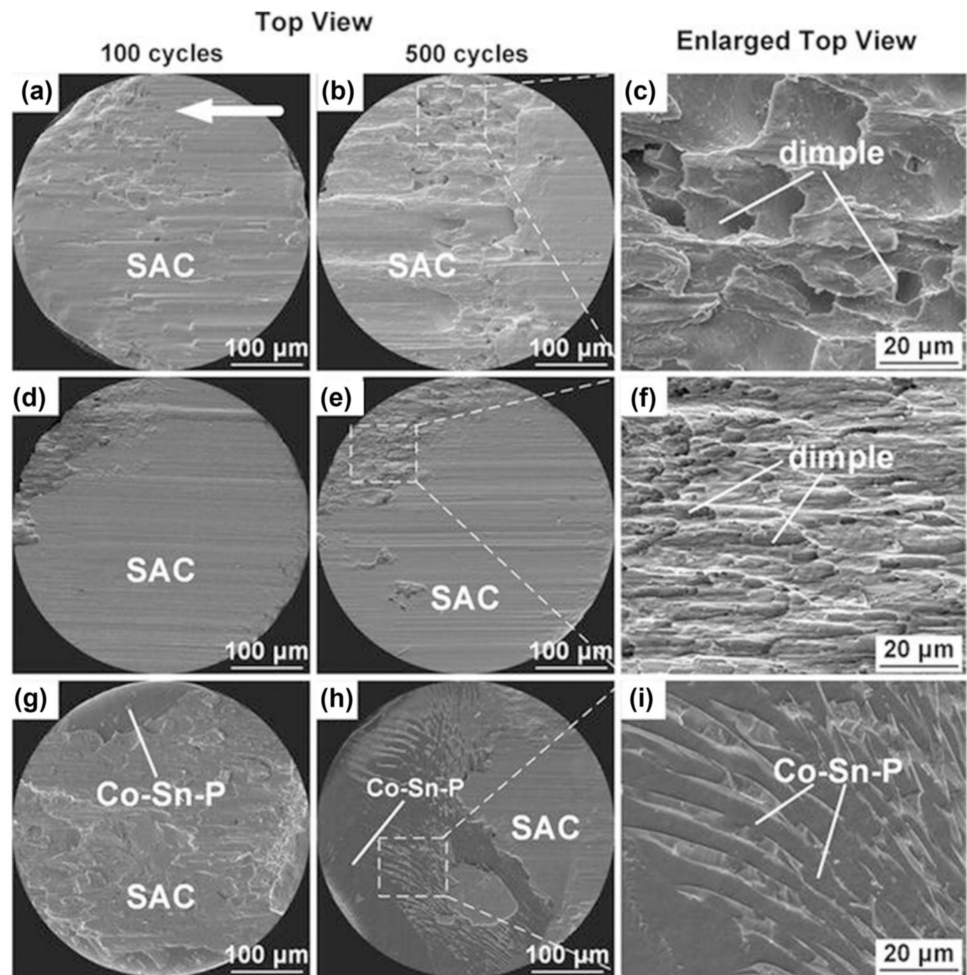

Fig. 12 SEM images of fractured surface of solder joints after 100 and 500 thermal cycles. **a**–**c** SnAgCu/Cu joints, **d**–**f** SnAgCu/Co–4 wt % P joints. **g**–**i** SnAgCu/Co–8 wt % P joints [85]

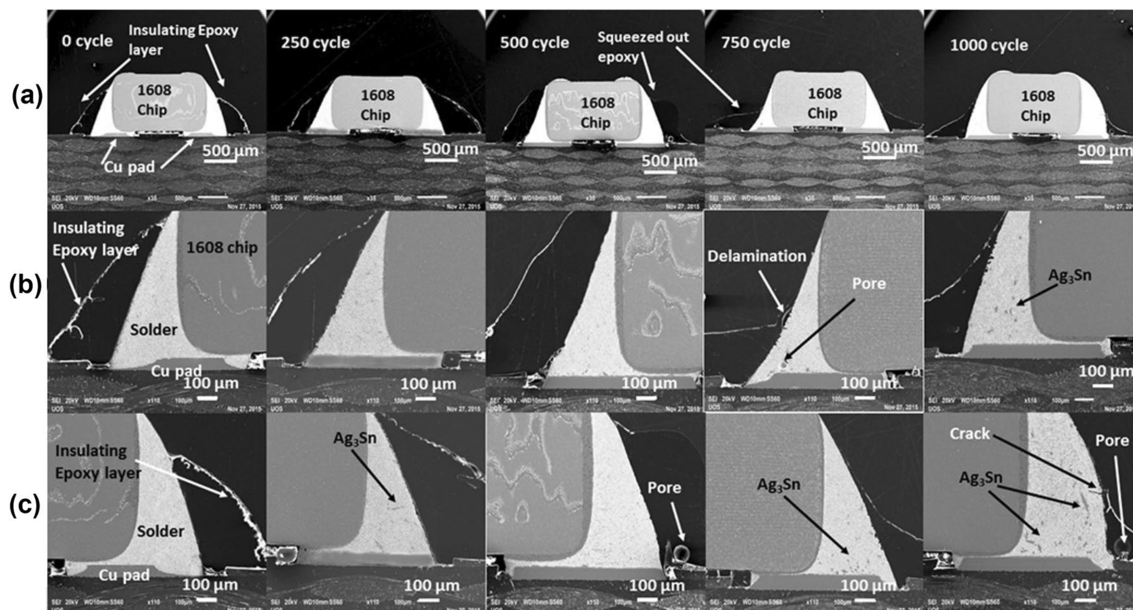

Fig. 13 Cross-section of solder joint after thermal cycling: **a** full view, **b** left side, **c** right side [88]

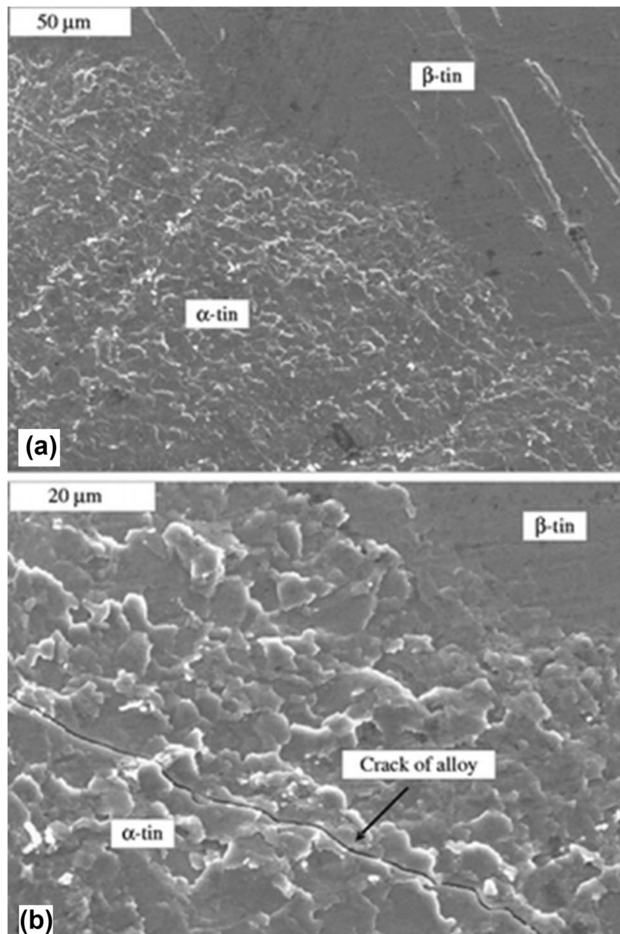

Fig. 14 SEM images of surface of Sn-1Cu solder alloy after long-term cryogenic storage: **a** boundary of α/β-Sn and **b** crack along α-Sn [89]

and Sb was higher than original solder matrix due to the strengthening effect of solute element and after long-term cryogenic storage, no tin pest was observed in modified solder alloy [92]. The addition of Ag could form small Ag_3Sn particle and meanwhile finer Cu_6Sn_5 particle was obtained in solder matrix, which helped to suppress tin pest formation. However, Cu had adverse effect on the cryogenic reliability of solder and the increasing content of α-Sn was observed with the addition of Cu in SnAgCu solder matrix [93]. As illustrated in Fig. 15, the α-Sn content of solder alloy containing Ag was lower than others after 4 days cryogenic treatment while the α-Sn was observed obviously in Sn–1Cu and Sn–3Cu solder. Moreover, compared to Sn-based solder alloy, In-based solder alloy is seen as an ideal electronic packaging materials for the cryogenic structure owing to its excellent cryogenic performance and some kinds of In-based solder alloys have been applied in the manufacture of satellite currently [94, 95]. However, the high cost of Indium limited the commercial application and its low melting temperature could not endure the wide-range change of service temperature of on-orbit satellite without active thermal control system. Up to now, researches on the evolution of lead-free solder joints subjected to extremely cryogenic environment are relatively absent and the further investigation to improve the reliability is required.

5 Electromigration

5.1 Influence mechanism

5.1.1 SnAgCu solder alloy

Under the drive of increasingly finer pitch of electronic devices, the electric current density in solder joint is greatly increased, which makes the electromigration of solder joint a serious reliability issue [96–98]. Once the current density reaches to the threshold of damaging electromigration, which is usually thought to be 1×10^4 A/cm^2, energetic atoms are generated and migrate parallel with the electron flow, resulting in the microstructure deterioration [99, 100]. Bashir et al. [101] found that after only 1000 h test at a constant current of 5 A, the IMC layer of SnAgCu solder joint at cathode side was attenuated with the formation of cracks near interface while the layer at the anode was greatly increased due to the diffusion of Cu atoms along the electron flow.

5.1.2 SnBi solder alloy

SnBi solder alloy is usually considered to be more sensitive to high-density current than other Sn-based solders, which limits the extensive application of SnBi solder alloy [102]. Not only coarsening interfacial layer but also the phase inhomogeneity could be observed in the SnBi/Cu solder joint during electromigration test [74]. As shown in Fig. 16, the formation of Bi-rich/Sn-rich layer at anode/cathode side respectively, was observed between solder matrix and the coarsening IMC layer after long-term electromigration at ambient temperature for only 336 h, which was ascribed to the atomic migration of Bi induced by high-density current [103]. With the segregation process of Bi and Sn, the mechanical property was decreased due to the brittle Bi-rich layer and the cracks were much easier to initiate and expand at the interface of solder joint. Moreover, the electrical resistivity of Bi was higher than other phase of SnBi solder joint and hence the coarsening Bi-rich layer gave a great decrease of electrical conductivity [104].

5.1.3 SnZn solder alloy

It has been reported that high-density current stress possessed a reverse polarity effect on the SnZn solder joint,

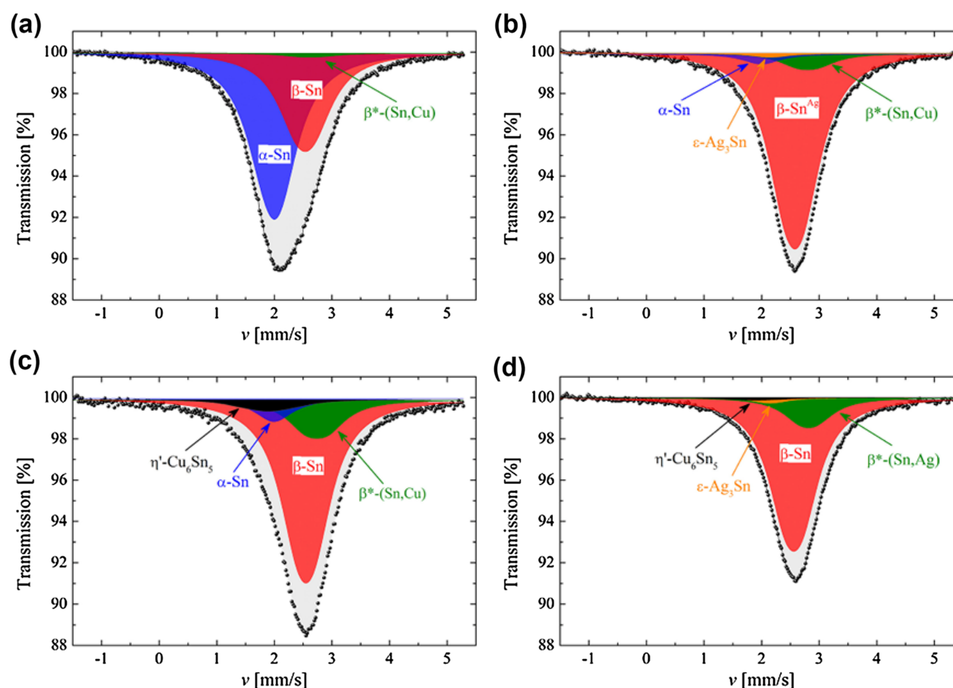

Fig. 15 Sn transmission Mössbauer spectra of **a** Sn–1Cu, **b** Sn–0.3Ag–0.7Cu, **c** Sn–3Cu and **d** Sn–3Ag–0.5Cu solder alloys after cryogenic treatment [93]

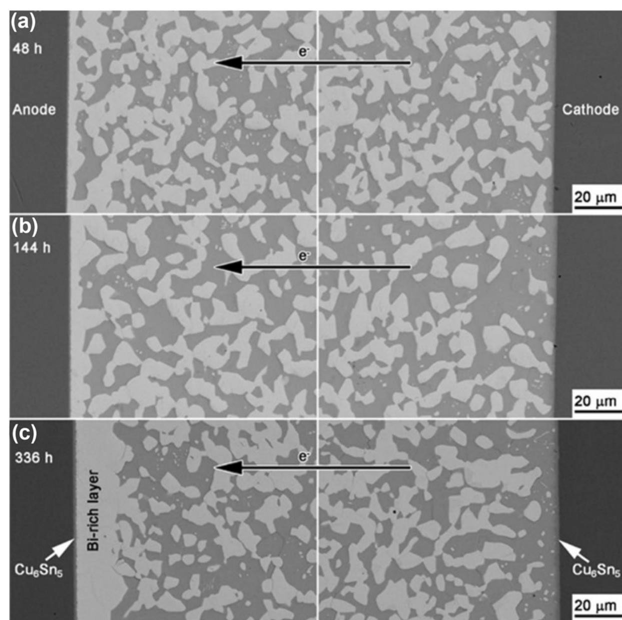

Fig. 16 BSE images on anode interfaces and cathode interfaces in Cu/Sn–58Bi/Cu solder joints after electromigration test with current density of 1.0×10^4 A/cm^2 at ambient temperature for **a** 48 h, **b** 144 h and **c** 336 h [103]

especially for the joint under thermoelectric stress [105, 106]. The Cu_5Zn_8 layer at the cathode side thickened more significantly than that at the anode side, which was ascribed to the opposite migration of Sn and Zn. Zhang et al. [107] found that after the electromigration at 4.26×10^4 A/cm^2 and 140 °C for 166 h, the thickness of interfacial layer at the cathode side was greatly increased with the dissolution of block-shaped Cu_5Zn_8 IMC into solder matrix. While at the anode side, the Cu_5Zn_8 layer was gradually replaced by a Cu_6Sn_5 layer, whose thickness was correspondingly thinner. Moreover, voids were observed at the cathodic IMC layer as well as the Zn-rich phase in the solder matrix due to the inhomogeneous migration of atoms induced by the electrical stress [106, 108]. With the increasingly higher service temperature of electronical device, the electromigration effect on solder joint is becoming more and more serious and should be concerned [109, 110]. Currently impeding atomic migration induced by electrical current is the main method to improve the electromigration-resistance of lead-free solder joint [111].

5.2 Micro-alloying

5.2.1 Rare earth elements

Compared to SnAgCu solder matrix, the grain of SnAgCu solder modified with Ce was finer and the $CeSn_3$ particles assembling at the grain boundary blocked the atomic diffusion, which hence retarded the formation of voids and cracks near interface [112]. Guo et al. [113] investigated the effect of RE addition on the reliability of SnBi solder joint under high-density current and found that Ce-La–Nd mixed RE could improve the electromigration resistance of SnBi solder joint. RE elements, accumulating at the grain boundaries of solder matrix, suppressed the grain boundary sliding and

resulted in the slower migration of Sn/Bi atoms in SnBi-RE solder joint. However, there were some researchers reported that under the same thermal-electrical stress, solder alloys doping with RE elements might perform worse than original solder matrix, which made the electromigration resistance of RE enhanced solder alloys an unclear issue [114, 115].

5.2.2 Other metallic elements

It was proved that the grain orientation of Sn matrix was one of the most critical factor in the serrated Cu dissolution at the cathode side, which was accelerated if the c-axis of Sn grain was parallel to the electron flow due to the lower activation energy of diffusion and resulted in the microstructure degradation [116–118]. The lifetime of SnAgBiIn solder joint modified with Co under high-density current stress was much longer than the original solder, which was attributed to the refinement effect of Co. The content of the Sn grain whose c-axis was parallel to the electron flow was reduced with the increasingly refined microstructure and hence the formation of voids and cracks induced by electromigration was retarded [119]. In some cases, the strengthening effect of alloying element is more obvious than nanoparticles even if their chemical compositions are all the same, which could be attributed to the aggregation of nanoparticles. Compared to SnBi solder joint doping with 0.4 Ag nanoparticles, the microstructure of SnBi–0.4Ag composite solder joint was much more uniform and refined, resulting in higher electromigration-resistance. Therefore, SnBi–0.4Ag composite solder joint performed best in the high-density current test among SnBi solder matrix and SnBi–0.4 nanoAg composite solder, as shown in Fig. 17 [120]. Wang et al. [121] fabricated a structural composite SnBi solder joint by adding a SnAgCu solder foil between two SnBi foils and found that the SnAgCu interlayer acted as a barrier layer which blocked the diffusion of Sn and Bi atoms. As a result, thinner IMC layer and Bi-rich layer without voids and cracks were obtained in the composite solder joint after electromigration test.

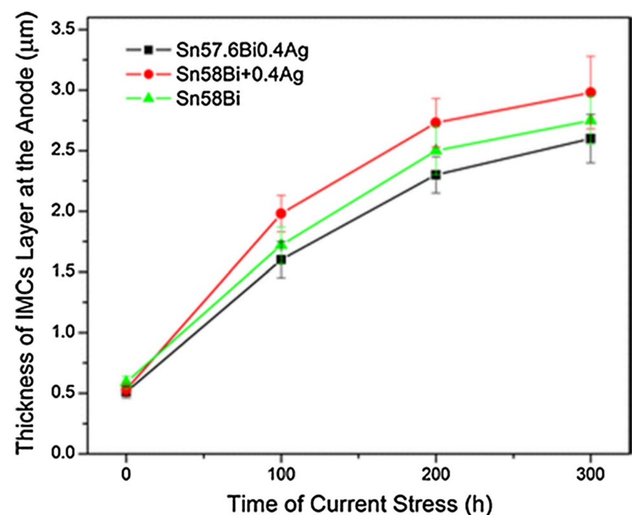

Fig. 17 The thickness evolution of Cu–Sn IMC layer at the anode side in SnBi0.4Ag, SnBi-0.4nanoAg and SnBi solder joint with the increasing time of current stress [120]

5.3 Nanoparticle strengthening

5.3.1 Metallic nanoparticles

Bashir et al. [101] found that the electromigration resistance of SnAgCu solder joint was improved when it was soldered by the Co nanoparticle-doped flux. Co nanoparticle could partly replace Cu atoms in IMC layer, forming $(Cu, Co)_6Sn_5$ IMC layer, and hence the diffusion of Cu induced by current stress was impeded. Moreover, as a barrier to the slide of dislocation and grain boundary, uniform Co nanoparticle retarded the formation of voids and cracks, stabilizing the microstructure of solder joint. But compared with Co nanoparticle, the strengthening effect of Ni nanoparticle was more obvious and after long-term electromigration test at the same parameter, the tensile strength of SnAgCu-nano Ni solder joint was higher than SnAgCu-system solder, as listed in Table 2 [122–124].

5.3.2 Compound nanoparticles

Nano Al_2O_3 could not only greatly reduce the diffusion coefficient of the elements, but also assemble at the grain boundary, acting as an barrier to the diffusion of atoms, and suppress the growth of Bi-rich layer and IMC layer of SnBi solder joint under current aging [125]. Kim et al. [3] investigated the effect of SiC nanoparticle addition on the electromigration resistance of SnAgBiIn solder joint and found that during high-density current test, only narrow voids were generated in the composite solder joint rather than obvious cracks, which prevented the current crowding.

5.3.3 Advanced nanoparticles

In comparison with plain SnZnBi solder alloy, doping with GNSs gave a strength increase of nearly 11% for the composite solder joint under the same electrical stress, which was ascribed to the much finer microstructure [126]. CNTs refined the microstructure of lead-free solders joints and bonded well with the solder matrix, sliding out of the bonding interface to relieve the stress under external load [127]. At the same time, doping CNTs could form a high conductive net in the solder matrix, which was the prior channel for the electron flow, and hence lower electromigration damage was obtained [128]. Moreover,

Table 2 The tensile strength of nano Ni-doped solder joint and its correlation with literature before/after electromigration [122]

Solder composition	Electromigration parameters	Tesile strength (MPa)		References
		Before	After	
Sn-3Ag-0.5Cu + nanoNi	$J = 5 \times 10^3$ A/cm^2 T = 150 °C t = 192 h	100.99 ± 4.2	77.23 ± 3.4	[122]
Sn-3Ag-0.5Cu	$J = 5 \times 10^3$ A/cm^2 T = 150 °C t = 192 h	60.34 ± 1.5	22.36 ± 8	[101]
Sn-3.8Ag-0.7Cu	$J = 5.03 \times 10^3$ A/cm^2 T = 145 °C t = 48 h	47	17	[123]
Sn-3.8Ag-0.7Cu	$J = 3 \times 10^4$ A/cm^2 T = 145 °C t = 98.5 h	55	35	[124]
Sn-3Ag-0.5Cu + nanoCo	$J = 5 \times 10^3$ A/cm^2 T = 150 °C t = 192 h	88.18 ± 1	78.16 ± 5.6	[101]

Ag-coated multi-walled CNTs could significantly improve the lifetime of SnBi solder joint due to the strengthening effect of uniform CNTs and nano-scale Ag_3Sn particle [129].

5.4 Enhanced substrate

As a barrier for the Cu diffusion, Ni surface provided a better electromigration resistance for solder joint but at a high current density of over 2000 A/cm^2, the consumption of Ni into solder matrix induced the current stress was observed, which weakened the reliability of solder joint again [130, 131]. The atomic electromigration flux of Bi (J_{em}) induced by current stress in SnBi solder joint could be expressed as follows [132]:

$$J_{em} = C\frac{D \times Z^*}{kT}e\rho j \tag{3}$$

where C, D, and Z* are the concentration, diffusivity and effective charge number of the diffusing Bi. ρ is the resistivity of SnBi solder and k is Boltzmann's constant. Compared to Cu pad, ENIG surface reduced the value of $D \times Z^*$ and hence lower atomic flux and higher electromigration-resistance were obtained, as listed in Table 3 [133]. (Pd, Ni)Sn_4 layer with low Ni content, forming at the interface of solder matrix and ENEPIG surface, could effectively retard the electromigration and consumption of Ni layer because $PdSn_4$ phase was more insusceptible to electromigration [134]. However, at the same electromigration test parameters, SnBi solder joint with OSP surface performed better than other films, which was ascribed to its highest activation energy for electromigration, as shown in Fig. 18 [135]. Therefore, it might indicate that OSP was an excellent surface for the lead-frees solder joint subjected to high-density current [136]. As the solder joint of electronical device is becoming increasingly finer, the electromigration damage has been unprecedentedly critical and further investigations to improve electromigration-resistance are necessary.

6 Corrosion

6.1 Influence mechanism

6.1.1 SnAgCu solder alloy

Other than providing electronical interconnection between devices, mechanical bonding is also an important function of solder joint. However, the increasingly wide application of solder alloy makes it easier to be exposed directly to the corrosion medium [137, 138]. Corrosion conditions, such as brackish coastal and humid conditions, act as the electrolyte and accelerate the corrosion process of solder matrix, which has become a major reason of joint failure [139]. As NaCl is one of the main corrosion medium for materials, the experiments to evaluate the corrosion resistance of solder alloy were usually conducted in the NaCl solution [140, 141]. The corrosion process of SnAgCu solder joint in the salt spray test is relatively simple, which could be clarified by the following galvanic corrosive reaction [142, 143]:

Table 3 D × Z* values at different test parameters for Sn-58Bi/Cu and Sn-58Bi/ENIG solder joint [133]

Test parameters (A/cm^2)	Substrate	J_{em}(atoms/cm^{2}s)	$D \times Z^*$(cm^2/s)
30 °C, 5×10^3	Cu	7.43×10^{12}	1.07×10^{-10}
30 °C, 5×10^3	ENIG	3.83×10^{12}	3.07×10^{-11}
75 °C, 5×10^3	Cu	1.84×10^{13}	2.87×10^{-10}
75 °C, 5×10^3	ENIG	1.24×10^{13}	1.77×10^{-10}

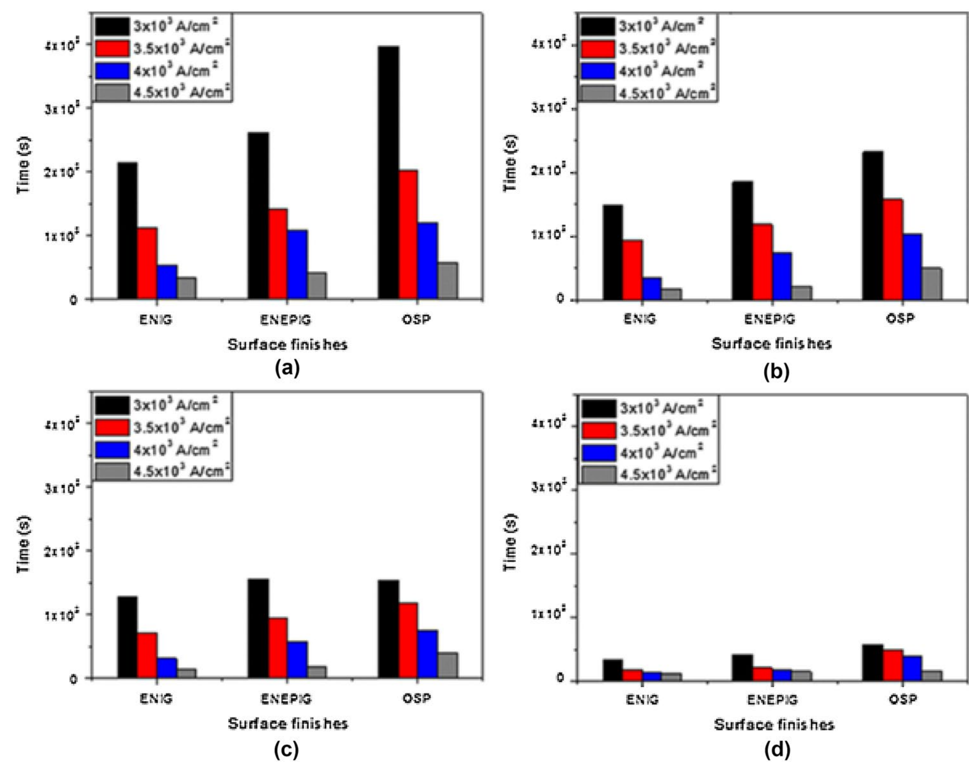

Fig. 18 The lifetime of Sn-58Bi solder joint with different surface at different parameters: **a** 80 °C, **b** 90 °C, **c** 100 °C and **d** 110 °C [135]

Cathodic reaction:

$$O_2 + 2H_2O + 4e^- = 4OH^- \quad (4)$$

Anodic reaction:

$$Sn + 2OH^- - 2e^- = SnO + H_2O \quad (5)$$

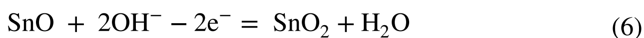

$$SnO + 2OH^- - 2e^- = SnO_2 + H_2O \quad (6)$$

Therefore, the dissolution of Sn matrix and the formation of oxide surface film with cracks were obtained, which gave a great decrease of joint strength [144]. What's more, the large IMC particle in solder matrix with higher electrochemical stability, such as Ag_3Sn and Cu_6Sn_5, could act as the excessive cathode area and accelerate the reaction process [145]. Moreover, current investigations proved that corrosion behavior of solder joint also aroused the growth of Sn whisker [146, 147]. The volume swelling induced by the corrosion products, increased the inner stress of solder joint and hence provided the growth energy of Sn whisker, which was an important reason for short circuit [148]. But in summary, it has been reported that the corrosion resistance of SnAgCu solder alloy is higher than SnBi and SnZn solder alloy, the mechanism of which is clarified in the following sections [149].

6.1.2 SnBi solder alloy

In the corrosive environment, the Sn-rich and Bi-rich phases in the solder matrix formed a large number of micro-scale galvanic cells where Sn-rich phase acted as the anode and Bi-rich phase acted as cathode [150]. With the progress of corrosion, Sn-rich phase was corroded, forming the pitting corrosion, and only Bi-rich phase remained, the high brittleness of which made the corrosion area lose the excellent mechanical properties [151, 152]. Mostofizadeh et al. [153] found that after long-term salt spray test, Sn-rich phase of SnBi solder joint was corroded away, forming the pitting corrosion, and dense Bi phase was observed. All corroded solder joints performed badly in the sequential drop test with the different fracture behavior from ductile mode to brittle mode.

6.1.3 SnZn solder alloy

The corrosion behavior of SnZn solder joint is more complicated than other Sn-based solders due to the existence of erodible Zn-rich phase [154]. Zn element with high chemical activity, is sensitive to the corrosion medium and easy to result in the pitting corrosion [155]. In the corrosive conditions, external Zn-rich phase was preferentially dissolved and hence a crack formed from the surface to solder matrix, which provided an accelerated path to the transport of corrosive medium and promote the corrosion process [156]. SEM observation and element mapping analysis showed that after corrosion test, corrosive medium migrated into Sn-12Zn solder matrix and micro-cracks formed along the intergranular boundary between Zn-rich phase and Sn, with inner-growing pits, as showed in Fig. 19 [157]. In general,

although SnZn solder alloy has a remarkable advantage in the melting temperature and cost, it performed the worst in the corrosive conditions in the current commercial Sn-based solders, which became a menace to its application [149].

6.2 Micro-alloying

6.2.1 Rare earth elements

In the melting SnZnLa solder, La could also help to form high melting-temperature IMC particles, which acted as the nucleation particles and hence reduced the average size of Zn-rich phase. As a result, SnZnLa solder alloy possessed a higher corrosion-resistance than SnZn solder [17]. As mentioned above, rare earth element could refine the microstructure of solder joint, which also help to improve its reliability under corrosion conditions. In Sn–3.5Ag solder matrix, large Sn grains and a sparse precipitate at the grain boundary while Sn3.5Ag-Ce showed more homogeneous distribution and smaller grain without coarsening IMC and hence the corrosion potential was decreased. Moreover, higher pitting resistance was obtained in Sn3.5Ag-Ce solder joint because a passive Ce oxide film mixed with Sn and Ag oxide formed at the surface of solder joint, which prevented the penetration of corrosive ion [158].

6.2.2 Other metallic elements

In the NaCl solution corrosion test, Sn0.5Cu solder alloy performed better than Sn3.0Ag solder alloy and no obvious cracks were observed on the surface of Sn0.5Cu solder alloy, which was attributed to the lower content of IMC in

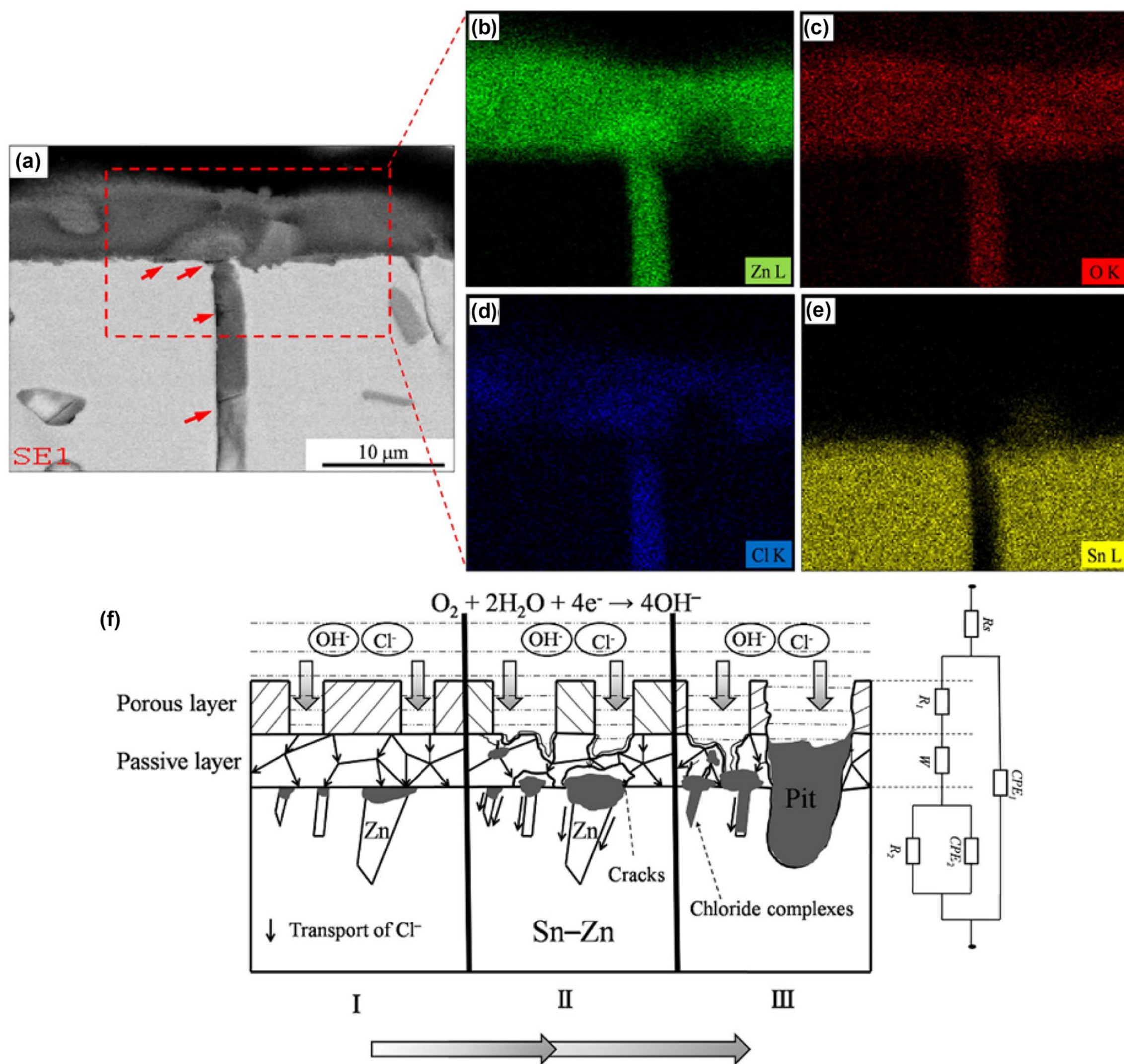

Fig. 19 SEM image of the cross-section (**a**) and the element mapping for Sn–12Zn solder alloy after corrosion test: **b** Zn, **c** O, **d** Cl, **e** Sn and **f** the schematic illustration of pitting corrosion process [157]

the Sn0.5Cu [159]. It has been proved the micro-galvanic corrosion between the cathodic coarsening IMCs and the anodic Sn matrix is one cause of corrosion and the large-platelet IMC could accelerate the corrosion process [160]. Therefore, decreasing the size and amount of IMC seems to be an effective method to improve the corrosion resistance of solder joint [161–163]. Compared to SnZn solder alloy, a thinner and more uniform passivation layer formed at the surface of SnZn-In solder along with smaller cracks and pits, which suppressed the migration of corrosive medium into matrix and improved the corrosion resistance of solder joint, as shown in Fig. 20 [164]. The addition of Ti promoted the formation of nuclei, giving a finer Zn-rich phase, and hence the probability of corrosion reaction was reduced [165]. The corrosion resistance of SnZn solder could be significantly improved by doping trace amount of Cr, which was ascribed to the formation of a compact and uniform passivation film on the surface, but the enhancing effect was unobvious until the content of Cr reached to 0.3 wt% [166]. The addition of Ni could only stabilize the passive film on the surface of SnZn solder joint to impede the migration of corrosive ions, but also lead to the formation of Ni_5Zn_{21} IMC particle, which promoted the refinement of Zn-rich phase [167]. Thus, as illustrated in Fig. 21, SnZn solder containing Ni showed a better corrosion resistance than SnZn solder containing other elements.

6.3 Nanoparticle strengthening

In the past decades, the investigations on enhancing the corrosion resistance of solder joint was concentrated on micro-alloying whereas the effect of nanoparticles addition was hardly covered. But actually, nanoparticles are also conducive to improving the reliability of lead-free solder joint subjected to corrosive medium [168].

The addition of CeO_2 nanoparticle refined Ag_3Sn IMC, decreasing the probability of galvanic corrosion, and enhanced the passivation film of solder matrix, which acted as a barrier to the corrosion propagation [169]. Therefore, the corrosion resistance of SnAg solder joint was significantly increased with lower corrosion current and corrosion potential. Wu et al. [170] investigated the effect of Al_2O_3 nanoparticle addition on the corrosion resistance of SnAgCu solder joint and found that the passive film on the surface of Sn–0.3Ag–0.7Cu–0.12Al_2O_3 was more homogeneous and compact than SnAgCu matrix, which could impede further corrosion. After long-term corrosion in NaCl solution, a quantity of pitting formed on the surface of SnAgCu solder joint whereas the surface of SnAgCu-nano Al_2O_3 still kept dense and compact due to the enhanced effect of aggregated nano Al_2O_3 on the surface, as shown in Fig. 22. Compared to SnBi solder alloy, the size of deep ditches of SnBi-nanoCu_6Sn_5 composite solder alloy induced by corrosion greatly shrunk because there were more boundaries in the composite solder, which acted as barriers for corrosive medium and reduced the corrosion rate, as shown in Fig. 23 [151]. The increasing corrosion resistance was also obtained in the Sn–3.5Ag–0.7Cu solder alloy containing Ni-CNTs. The finer Sn matrix and Ag_3Sn induced by the dispersing Ni-CNTs, formed quantities of corrosion microcells and Ni-CNTs could act as the electrode [171]. Therefore, the galvanic corrosion between the Sn anode and Ag_3Sn cathode

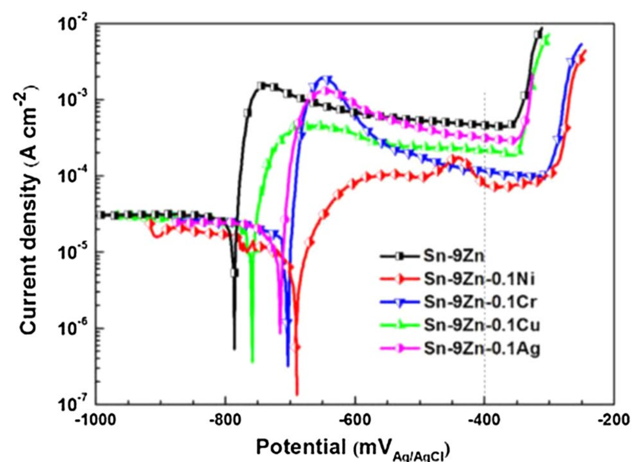

Fig. 21 Polarization curves of alloys in NaCl 3.5 wt % solution [167]

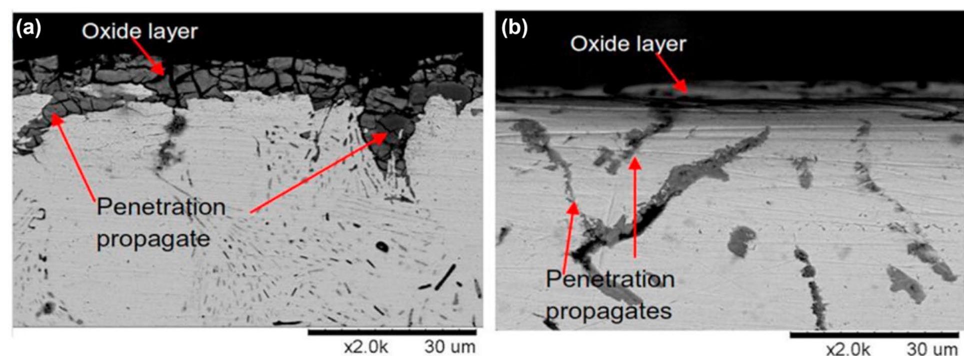

Fig. 20 Cross-sectional morphologies of (**a**) Sn–9Zn and (**b**) Sn–9Zn–4In solder alloys after corrosion test [164]

in the Sn–3.5Ag–0.7Cu solder alloy containing Ni-CNTs was reduced.

7 Irradiation

In addition to extremely cryogenic temperature, the cosmic radiation consisting of γ-ray, energetic proton and cosmic ray, is another severe barrier to the on-orbit satellite [172, 173]. Energetic radiation particles could cause supersaturated micro-defects in the satellite material along with the degradation of properties [174–176]. Compared to structural materials, the electronic material is much more vulnerable to the irradiation and hence currently radiation-shielding devices are generally applied to prevent the electronic system from irradiation damage [177]. Unfortunately, the radiation-shielding devices increase the weight of satellite and fail to meet the light-weighting demand of deep space mission. After long-term interplanetary travel, it is important for satellite to reduce its velocity to enter the orbit of the target planet rather than fly by to carry out more exploration mission. The quantity of fuel used to change the velocity could be calculated by the Tsiolkovsky's rocket equation [178]:

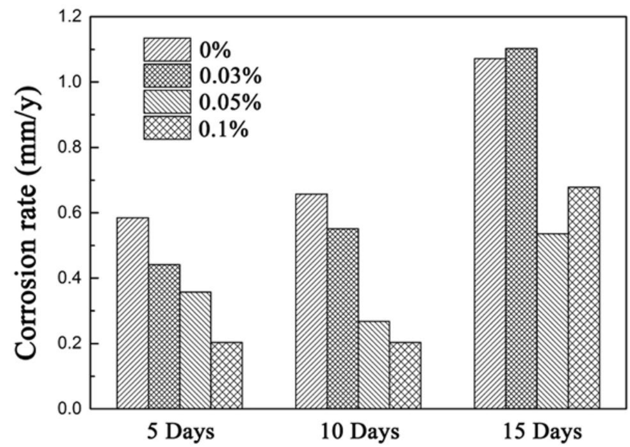

Fig. 23 Comparisons in corrosion rate of composite solder with different Cu_6Sn_5 nanoparticle concentrations [151]

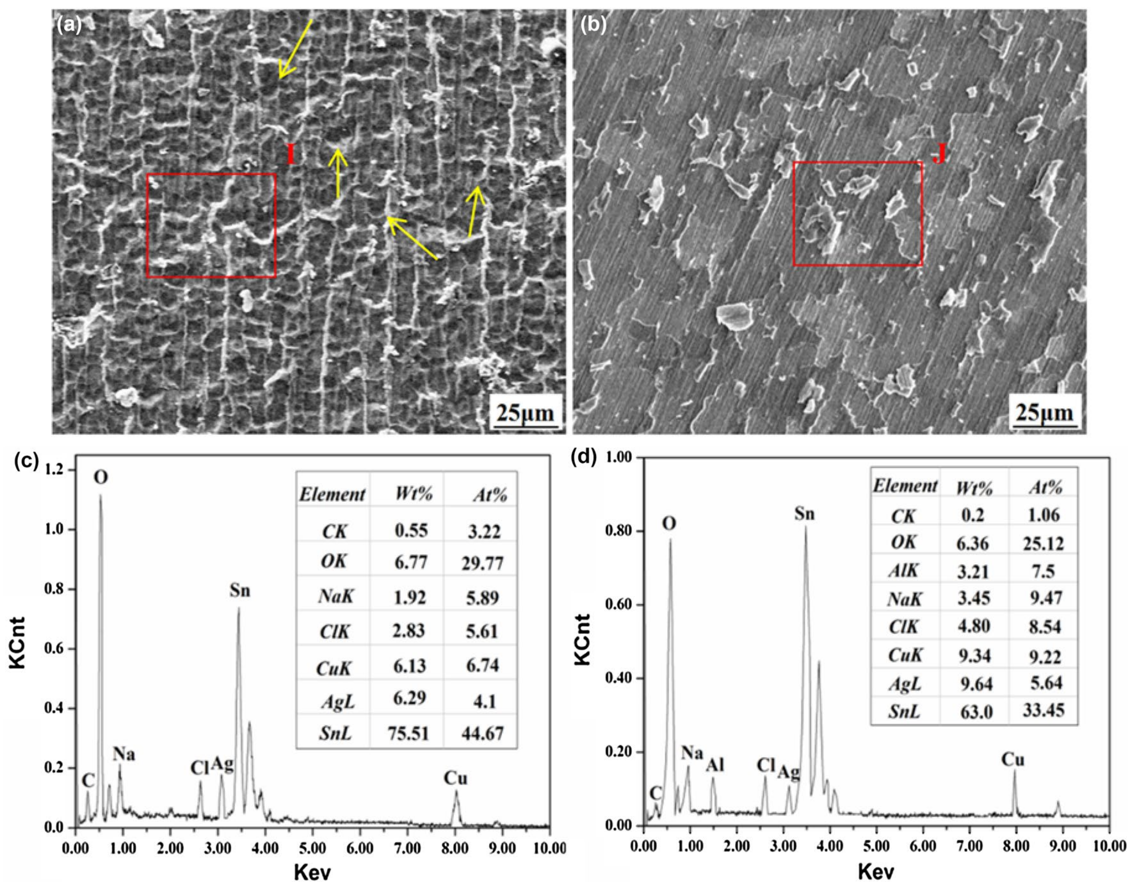

Element	Wt%	At%
CK	0.55	3.22
OK	6.77	29.77
NaK	1.92	5.89
ClK	2.83	5.61
CuK	6.13	6.74
AgL	6.29	4.1
SnL	75.51	44.67

Element	Wt%	At%
CK	0.2	1.06
OK	6.36	25.12
AlK	3.21	7.5
NaK	3.45	9.47
ClK	4.80	8.54
CuK	9.34	9.22
AgL	9.64	5.64
SnL	63.0	33.45

Fig. 22 SEM image of **a** SnAgCu and **b** SnAgCu-0.12Al_2O_3 solders after corroded in 0.1 M NaCl for 30 days; **c** EDS analysis of region I in (**a**); **d** EDS analysis of region J in (**b**) [170]

$$\Delta v = v_e \ln \frac{m_0}{m_1} \quad (7)$$

where Δv is the maximum disparity of velocity, v_e is the effective exhaust velocity, m_0 is the initial total mass and m_1 is the mass without propellant ($m_0 - m_{fuel}$). A small increment of weight would significantly increase the requirement of the fuel, which is unable to support the increasingly wider range and more complex mission of deep space exploration. Therefore, many importance has been attached to improving the reliability of electronic materials exposed directly to cosmic radiation environment. However few researches on the irradiation effect on the reliability of lead-free solder joints have been reported and only the investigation on the reliability of lead-containing solder joint subjected to gamma-ray irradiation has been conducted, in which the decreasing properties was obtained [179]. With the development of aerospace industry, it is meaningful to clarify the effect of cosmic radiation on the lead-free solder joint to explore to reduce the radiation-shielding devices and provide the reference for the design of next-generation satellite.

8 Conclusions

In the past decades, quantities of researches have been conducted to clarify the reliability evolution of lead-free solder alloy exposed to several special environments and many novel lead-free solder alloy systems have been created under the drive of environment-friendly development. However, it should be noted that the current reliability researches on the lead-free solder alloy are mainly focused on the thermo-electrical challenge, which is hardly comprehensive due to the increasingly severe service environment of solder joint. More investigations on the reliability of lead-free solder joint subjected to corrosive, cosmic or multi-field coupling conditions are needed to provide the reference for the design of future packaging materials. Moreover, it could be concluded that the enhancement of micro-alloying is not effective enough to meet the property demand of novel solder alloy. Although the reliability improvement could be obtained in the solder joint doping with nanoparticles, the composite solder alloy is still stuck on the plateau of academic research and is far away from industrial application because of its high-budget preparation. It may be significant to explore to enhance the reliability of lead-free solder alloy by the composite addition of element and nanoparticles, which is seen as an effective method to design the future solder alloy with excellent reliability. Besides, the substrate enhancement also shows a great potential to increase the reliability and is much easier to be applied in the electrical industry compared with micro-alloying and doping nanoparticles. In summary, this review concentrates on the recent reliability investigations on lead-free solder alloy and tries to provide theoretical support for the design of reliable electrical packaging materials. With the advance of electronical technology, more researches on the solder alloy are expected to contribute to complying with the increasing requirement of electrical industry in the near future.

Acknowledgement This research was supported by the National Natural Science Foundation of China (Grant NO. 51675269) and the Priority Academic Program Development of Jiangsu Higher Education Institutions(PAPD).

References

1. L. Zhang, K.N. Tu, Mater. Sci. Eng., R **82**, 1 (2014)
2. Y. Yao, X. Li, X. He, J. Mater. Sci.: Mater. Electron. **29**, 4517 (2018)
3. Y. Kim, S. Nagao, T. Sugahara, K. Suganuma, M. Ueshima, H.-J. Albrecht, K. Wilke, J. Strogies, J. Electron. Mater. **43**, 4428 (2014)
4. U.S. Mohanty, K.-L. Lin, J. Electron. Mater. **42**, 628 (2013)
5. W.-R. Myung, Y. Kim, K.-Y. Kim, S.-B. Jung, J. Electron. Mater. **45**, 3651 (2016)
6. D. Li, C. Liu, P.P. Conway, J. Electron. Mater. **35**, 388 (2006)
7. W. Peng, M.E. Marques, J. Electron. Mater. **36**, 1679 (2007)
8. J. Wang, H. Nishikawa, Microelectron. Reliab. **54**, 1583 (2014)
9. W. Peng, E. Monlevade, M.E. Marques, Microelectron. Reliab. **47**, 2161 (2007)
10. Y. Liu, J. Meerwijk, L. Luo, H. Zhang, F. Sun, C.A. Yuan, G. Zhang, J. Mater. Sci.: Mater. Electron. **25**, 4954 (2014)
11. O. Mokhtari, H. Nishikawa, Mater. Sci. Eng., A **651**, 831 (2016)
12. T.Y. Kang, Y.Y. Xiu, C.Z. Liu, L. Hui, J.J. Wang, W.P. Tong, J. Alloys Compd. **509**, 1785 (2011)
13. P.J. Shang, L. Zhang, Z.Q. Liu, J. Tan, J.K. Shang, Microelectron. Reliab. **53**, 899 (2013)
14. H.F. Zou, Q.K. Zhang, Z.F. Zhang, Scr. Mater. **61**, 308 (2009)
15. T.Y. Kang, Y.Y. Xiu, L. Hui, J.J. Wang, W.P. Tong, C.Z. Liu, J. Mater. Sci. Technol. **27**, 741 (2011)
16. K. Suganuma, K. Niihara, T. Shoutoku, Y. Nakamura, J. Mater. Res. **13**, 2859 (1998)
17. L. Zhang, J. Han, Y. Guo, C. He, IEEE Trans. Electron. Dev. **59**, 3269 (2012)
18. J. Hu, A. Hu, M. Li, D. Mao, Mater. Charact. **61**, 355 (2010)
19. P. Xue, S.-B. Xue, Y.-F. Shen, H. Zhu, Mater. Des. **60**, 1 (2014)
20. W. Chen, S. Xue, H. Wang, Y. Hu, J. Wang, J. Mater. Sci.: Mater. Electron. **21**, 719 (2010)
21. L. Gao, S. Xue, L. Zhang, Z. Sheng, G. Zeng, F. Ji, J. Mater. Sci.: Mater. Electron. **21**, 643 (2010)
22. X. Tu, D. Yi, J. Wu, B. Wang, J. Alloys Compd. **698**, 317 (2017)
23. W. Dong, Y. Shi, Z. Xia, Y. Lei, F. Guo, J. Electron. Mater. **37**, 982 (2008)
24. P. Xue, S.-B. Xue, Y.-F. Shen, F. Long, H. Zhu, J. Mater. Sci.: Mater. Electron. **25**, 4219 (2014)
25. H. Wang, S. Xue, J.X. Wang, J. Mater. Sci.: Mater. Electron. **28**, 1 (2017)
26. S. Mukherjee, A. Dasgupta, B. Zhou, T.R. Bieler, J. Electron. Mater. **43**, 1119 (2014)
27. M. Ghosh, M.K. Gunjan, S.K. Das, A. Kar, R.N. Ghosh, A.K. Ray, Mater. Sci. Technol. **26**, 610 (2010)

28. M. Hasnine, N. Vahora, J. Mater. Sci.: Mater. Electron. **29**, 8904 (2018)
29. B. Ali, M.F.M. Sabri, N.L. Sukiman, I. Jauhari, J. Mater. Sci.: Mater. Electron. **28**, 197 (2017)
30. J. Zhao, L. Qi, X.-M. Wang, L. Wang, J. Alloys Compd. **375**, 196 (2004)
31. F.Q. Hu, Q.K. Zhang, J.J. Jiang, Z.L. Song, Mater. Lett. **214**, 142 (2018)
32. L. Yang, W. Zhou, Y. Ma, X. Li, Y. Liang, W. Cui, P. Wu, Mater. Sci. Eng., A **667**, 368 (2016)
33. Y. Tang, S.M. Luo, W.F. Huang, Y.C. Pan, G.Y. Li, J. Alloys Compd. **719**, 365 (2017)
34. Y. Tang, S.M. Luo, Z.H. Li, C.J. Hou, G.Y. Li, J. Electron. Mater. **47**, 5913 (2018)
35. L.C. Tsao, J. Alloys Compd. **509**, 2326 (2011)
36. B. Guo, A. Kunwar, N. Zhao, J. Chen, Y. Wang, H. Ma, Mater. Res. Bull. **99**, 239 (2018)
37. Z.L. Li, L.X. Cheng, G.Y. Li, J.H. Huang, Y. Tang, J. Alloys Compd. **697**, 104 (2017)
38. A. Sharma, A.K. Srivastava, K. Lee, B. Ahn, Metal Mater. Int. **5**, 4 (2019). https://doi.org/10.1007/s12540-019-00250-1
39. C. Peng, J. Shen, H. Yin, J. Mater. Sci.: Mater. Electron. **24**, 203 (2013)
40. Y. Ma, X. Li, W. Zhou, L. Yang, P. Wu, Mater. Des. **113**, 264 (2017)
41. F. Khodabakhshi, R. Sayyadi, N.S. Javid, Mater. Sci. Eng., A **702**, 371 (2017)
42. D. Ma, P. Wu, J. Alloys Compd. **671**, 127 (2016)
43. L. Yang, W. Zhou, X. Li, Y. Ma, Y. Liang, W. Cui, P. Wu, J. Mater. Sci.: Mater. Electron. **27**, 12264 (2016)
44. J.W. Jang, S.J. Yoo, H.I. Hwang, S.Y. Yuk, C.K. Kim, S.J. Kim, J.S. Han, S.H. An, J. Electron. Mater. **44**, 3957 (2015)
45. M. Sona, K.N. Prabhu, J. Electron. Mater. **45**, 3744 (2016)
46. H.-K. Cheng, Y.-J. Lin, C.-M. Chen, K.-C. Liu, Y.-L. Wang, T.-F. Liu, Metall. Mater. Trans. A **47**, 3971 (2016)
47. F.-J. Chen, S. Yan, Z.-G. Yang, Solder Surf. Mt. Technol. **26**, 180 (2014)
48. J.-W. Yoon, B.-I. Noh, S.-B. Jung, J. Electron. Mater. **40**, 1950 (2011)
49. C. Huang, L. Rao, M. Sun, A. Hu, M. Li, J. Electron. Mater. **48**, 1 (2019)
50. W.H. Wu, C.S. Lin, S.H. Huang, C.E. Ho, J. Electron. Mater. **39**, 2387 (2010)
51. Q. Zhang, H. Zou, Z.-F. Zhang, J. Mater. Res. **25**, 303 (2010)
52. C.-F. Tseng, K.-J. Wang, J.-G. Duh, J. Electron. Mater. **39**, 2522 (2010)
53. H. Chen, J. Han, J. Li, M. Li, Microelectron. Reliab. **52**, 1112 (2012)
54. E. Dalton, G. Ren, J. Punch, M.N. Collins, Mater. Des. **154**, 184 (2018)
55. D.A. Shnawah, M.F.M. Sabri, I.A. Badruddin, Microelectron. Reliab. **52**, 90 (2012)
56. J. Wang, S. Xue, Z. Lv, L. Wen, S. Liu, J. Mater. Sci.: Mater. Electron. **30**, 4990 (2019)
57. X. Li, F. Li, F. Guo, Y. Shi, J. Electron. Mater. **40**, 51 (2011)
58. R. Tian, C. Hang, Y. Tian, L. Zhao, Mater. Sci. Eng., A **709**, 125 (2018)
59. R. Tian, C. Hang, Y. Tian, J. Feng, J. Alloys Compd. **777**, 463 (2019)
60. N.M. Poon, C.M.L. Wu, J.K.L. Lai, Y.C. Chan, IEEE Trans. Adv. Packaging **23**, 708 (2000)
61. Y. Zuo, L. Ma, S. Liu, Y. Shu, F. Guo, J. Electron. Mater. **44**, 597 (2015)
62. H.-W. Miao, J.-G. Duh, B.-S. Chiou, J. Mater. Sci.: Mater. Electron. **11**, 609 (2000)
63. G. Ren, I.J. Wilding, M.N. Collins, J. Alloys Compd. **665**, 251 (2016)
64. S. Liu, S.-B. Xue, P. Xue, D.-X. Luo, J. Mater. Sci.: Mater. Electron. **26**, 4389 (2015)
65. L. Zhang, L. Sun, Y.-H. Guo, C.-W. He, J. Mater. Sci.: Mater. Electron. **25**, 1209 (2014)
66. L. Zhang, S.B. Xue, G. Zeng, L.L. Gao, H. Ye, J. Alloys Compd. **510**, 38 (2012)
67. J. Wu, S. Xue, J. Wang, S. Liu, Y. Han, L. Wang, J. Mater. Sci.: Mater. Electron. **27**, 12729 (2016)
68. J. Shen, C. Wu, S. Li, J. Mater. Sci.: Mater. Electron. **23**, 156 (2012)
69. L. Zhang, J.G. Han, Y.H. Guo, C.W. He, Sci. Technol. Weld. Join. **17**, 424 (2012)
70. Y. Wang, X.C. Zhao, Y. Liu, J.W. Cheng, H. Li, X.C. Xie, Mater. Sci. Forum **815**, 109 (2015)
71. W.S. Hong, C. Oh, M.-S. Kim, Y.W. Lee, H.J. Kim, S.J. Hong, J.T. Moon, J. Electron. Mater. **45**, 6150 (2016)
72. Y. Zhong, W. Liu, C. Wang, X. Zhao, J.F.J.M. Caers, Mater. Sci. Eng., A **652**, 264 (2016)
73. A.K. Gain, L. Zhang, J. Mater. Sci.: Mater. Electron. **27**, 11273 (2016)
74. L. Yang, L. Zhu, Y. Zhang, S. Zhou, G. Wang, S. Shen, X. Shi, Mater. Charact. **148**, 280 (2019)
75. Z. Zhao, L. Liu, H.S. Choi, J. Cai, Q. Wang, Y. Wang, G. Zou, Microelectron. Reliab. **60**, 126 (2016)
76. Y. Wen, X. Zhao, Z. Chen, Y. Gu, Y. Wang, Z. Chen, X. Wang, J. Alloys Compd. **696**, 799 (2017)
77. Y. Gu, X. Zhao, Y. Li, Y. Liu, Y. Wang, Z. Li, J. Alloys Compd. **627**, 39 (2015)
78. P. Chen, X. Zhao, Y. Wang, B. Zheng, C. Liu, S. Chen, J. Mater. Sci.: Mater. Electron. **27**, 1507 (2016)
79. Y.D. Han, H.Y. Jing, S.M.L. Nai, L.Y. Xu, C.M. Tan, J. Wei, Intermetallics **31**, 72 (2012)
80. J. Han, P. Gu, L. Ma, F. Guo, J. Liu, J. Electron. Mater. **47**, 2479 (2018)
81. L. Ma, Y. Zuo, S. Liu, F. Guo, A. Lee, K.N. Subramanian, J. Alloys Compd. **657**, 400 (2016)
82. Y. Xia, X. Xie, J. Alloys Compd. **454**, 174 (2008)
83. C.J. Lee, W.-Y. Chen, T.-T. Chou, T.-K. Lee, Y.-C. Wu, T.-C. Chang, J.-G. Duh, J. Mater. Sci.: Mater. Electron. **26**, 10055 (2015)
84. L.-Y. Gao, Z.-Q. Liu, C.-F. Li, J. Electron. Mater. **46**, 5338 (2017)
85. D. Yang, J. Cai, Q. Wang, J. Li, Y. Hu, L. Li, J. Mater. Sci.: Mater. Electron. **26**, 962 (2015)
86. Y.-G. Sung, W.-R. Myung, H. Jeong, M.-K. Ko, J. Moon, S.-B. Jung, J. Electron. Mater. **47**, 4165 (2018)
87. J. Kim, W.-R. Myung, S.-B. Jung, J. Electron. Mater. **45**, 5895 (2016)
88. A. Sharma, Y.-J. Jang, J.B. Kim, J.P. Jung, J. Alloys Compd. **704**, 795 (2017)
89. A. Skwarek, M. Sroda, M. Pluska, A. Czerwinski, J. Ratajczak, K. Witek, Solder Surf. Mt. Technol. **23**, 184 (2011)
90. Tian R., Tian Y., Wang C. and Zhao L., Mater. Sci. Eng., A **684**, 697(2017)
91. J. Wang, X. Long, Y. Yao, J. Mater. Sci.: Mater. Electron. **28**, 14884 (2017)
92. M. Leodolter-Dworak, I. Steffan, W.J. Plumbridge, H. Ipser, J. Electron. Mater. **39**, 105 (2010)
93. P. Zachariasz, A. Skwarek, B. Illés, J. Żukrowski, T. Hurtony, K. Witek, Microelectron. Reliab. **82**, 165 (2018)
94. R.M. Panas, M.L. Culpepper, IEEE Trans. Electron. Dev. **62**, 1977 (2015)
95. E.E.M. Noor, H. Zuhailawati, O. Radzali, J. Mater. Sci.: Mater. Electron. **27**, 1408 (2016)

96. Y. Li, A.B.Y. Lim, K. Luo, Z. Chen, F. Wu, Y.C. Chan, J. Alloys Compd. **673**, 372 (2016)
97. Y.-W. Chang, Y. Cheng, L. Helfen, F. Xu, T. Tian, M. Scheel, M. Di Michiel, C. Chen, K.-N. Tu, T. Baumbach, Sci. Rep. **7**, 17950 (2017)
98. F. Wang, H. Chen, D. Li, Z. Zhang, X. Wang, Electron. Mater. Lett. **15**, 36 (2019)
99. C. Chen, H.M. Tong, K.N. Tu, Annu. Rev. Mater. Res. **40**, 531 (2010)
100. Y. Zuo, T.R. Bieler, Q. Zhou, L. Ma, F. Guo, J. Electron. Mater. **47**, 1881 (2018)
101. M.N. Bashir, A.S.M.A. Haseeb, A.Z.M.S. Rahman, M.A. Fazal, J. Mater. Sci. Technol. **32**, 1129 (2016)
102. F. Wang, H. Chen, Y. Huang, L. Liu, Z. Zhang, J. Mater. Sci.: Mater. Electron. **30**, 3222 (2019)
103. F. Wang, L. Liu, M. Wu, D. Li, J. Mater. Sci.: Mater. Electron. **29**, 8895 (2018)
104. J. Sun, G. Xu, F. Guo, Z. Xia, Y. Lei, Y. Shi, X. Li, X. Wang, J. Mater. Sci. **46**, 3544 (2011)
105. S.-M. Kuo, K.-L. Lin, J. Mater. Res. **22**, 1240 (2007)
106. X.F. Zhang, J.D. Guo, J.K. Shang, J. Mater. Res. **23**, 3370 (2008)
107. X.F. Zhang, J.D. Guo, J.K. Shang, Scr. Mater. **57**, 513 (2007)
108. T.-H. Wang, K.-L. Lin, J. Electron. Mater. **45**, 164 (2016)
109. W.-J. Chen, Y.-L. Lee, T.-Y. Wu, T.-C. Chen, C.-H. Hsu, M.-T. Lin, J. Electron. Mater. **47**, 35 (2018)
110. F. Wang, L. Liu, D. Li, M. Wu, J. Mater. Sci.: Mater. Electron. **29**, 21157 (2018)
111. F. Wang, D. Li, Z. Zhang, M. Wu, C. Yan, J. Mater. Sci.: Mater. Electron. **28**, 19051 (2017)
112. H.X. Xie, D. Friedman, K. Mirpuri, N. Chawla, J. Electron. Mater. **43**, 33 (2014)
113. H. He, G. Xu, F. Guo, J. Mater. Sci. **44**, 2089 (2009)
114. H.-J. Lin, J.-S. Lin, T.-H. Chuang, J. Alloys Compd. **487**, 458 (2009)
115. H.-J. Lin, T.-H. Chuang, Mater. Lett. **64**, 506 (2010)
116. Y. Tian, J. Han, L. Ma, F. Guo, Microelectron. Reliab. **80**, 7 (2018)
117. T.L. Yang, J.J. Yu, C.C. Li, Y.F. Lin, C.R. Kao, J. Alloys Compd. **627**, 281 (2015)
118. Y. Wang, Y. Wang, J. Han, S. Tan, F. Guo, J. Mater. Sci.: Mater. Electron. **29**, 5954 (2018)
119. Y. Kim, S. Nagao, T. Sugahara, K. Suganuma, M. Ueshima, H.-J. Albrecht, K. Wilke, J. Strogies, J. Mater. Sci.: Mater. Electron. **25**, 3090 (2014)
120. H. Sun, Y.C. Chan, F. Wu, J. Mater. Sci.: Mater. Electron. **26**, 5129 (2015)
121. F. Wang, L. Zhou, Z. Zhang, J. Wang, X. Wang, M. Wu, J. Electron. Mater. **46**, 6204 (2017)
122. M.N. Bashir, A.S.M.A. Haseeb, J. Mater. Sci.: Mater. Electron. **29**, 3182 (2018)
123. F. Ren, J.-W. Nah, K.N. Tu, B. Xiong, L. Xu, J.H.L. Pang, Appl. Phys. Lett. **89**, 141914 (2006)
124. L. Zhang, Z.G. Wang, J.K. Shang, Scr. Mater. **56**, 381 (2007)
125. T. Hu, Y. Li, Y.C. Chan, F. Wu, Microelectron. Reliab. **55**, 1226 (2015)
126. X. Hu, Y.C. Chan, K. Zhang, K.C. Yung, J. Alloys Compd. **580**, 162 (2013)
127. L. Yang, H. Liu, Y. Zhang, H. Yu, J. Mater. Eng. Perform. **26**, 6028 (2017)
128. Z. Yang, W. Zhou, P. Wu, J. Alloys Compd. **581**, 202 (2013)
129. J. Kim, K.-H. Jung, J.-H. Kim, C.-J. Lee, S.-B. Jung, J. Alloys Compd. **775**, 581 (2019)
130. T.C. Huang, T.L. Yang, J.H. Ke, C.H. Hsueh, C.R. Kao, Scr. Mater. **80**, 37 (2014)
131. C.K. Chung, Y.J. Chen, W.M. Chen, C.R. Kao, Acta Mater. **60**, 4586 (2012)
132. K.N. Tu, Phys. Rev. B **45**, 1409 (1992)
133. S. Ismathullakhan, H. Lau, Y.-C. Chan, Microsyst. Technol. **19**, 1069 (2013)
134. C.-H. Wang, K.-T. Li, J. Alloys Compd. **654**, 546 (2016)
135. S.-M. Lee, J.-W. Yoon, S.-B. Jung, J. Mater. Sci.: Mater. Electron. **27**, 1105 (2016)
136. J.-H. Kim, Y.-C. Lee, S.-M. Lee, S.-B. Jung, Microelectron. Eng. **120**, 77 (2014)
137. M. Abtew, G. Selvaduray, Mater. Sci. Eng., R **27**, 95 (2000)
138. D. Li, P.P. Conway, C. Liu, Corros. Sci. **50**, 995 (2008)
139. M. Wang, J. Wang, W. Ke, J. Mater. Sci.: Mater. Electron. **25**, 1228 (2014)
140. F. Rosalbino, E. Angelini, G. Zanicchi, R. Carlini, R. Marazza, Electrochim. Acta **54**, 7231 (2009)
141. L. Hua, C. Yang, Microelectron. Reliab. **51**, 2274 (2011)
142. M. Winnicki, A. Baszczuk, M. Rutkowska-Gorczyca, A. Małachowska, A. Ambroziak, Surf. Eng. **32**, 691 (2016)
143. H. Kang, M. Lee, D. Sun, S. Pae, J. Park, Scr. Mater. **108**, 126 (2015)
144. E.S. Freitas, W.R. Osório, J.E. Spinelli, A. Garcia, Microelectron. Reliab. **54**, 1392 (2014)
145. H. Wang, Z. Gao, Y. Liu, C. Li, Z. Ma, L. Yu, J. Mater. Sci.: Mater. Electron. **26**, 11 (2015)
146. B. Illés, B. Horváth, J. Alloys Compd. **616**, 116 (2014)
147. B. Horváth, B. Illés, T. Shinohara, G. Harsányi, Thin Solid Films **520**, 384 (2011)
148. B. Illés, T. Hurtony, B. Medgyes, Corros. Sci. **99**, 313 (2015)
149. S. Farina, C. Morando, J. Mater. Sci.: Mater. Electron. **26**, 464 (2015)
150. M. Mostofizadeh, J. Pippola, L. Frisk, J. Electron. Mater. **43**, 1335 (2014)
151. X. Li, Y. Ma, W. Zhou, P. Wu, Mater. Sci. Eng., A **684**, 328 (2017)
152. M. Mori, K. Miura, T. Sasaki, T. Ohtsuka, Corros. Sci. **44**, 887 (2002)
153. M. Mostofizadeh, J. Pippola, T. Marttila, L.K. Frisk, IEEE Trans. Comp. Pack. Manf. **3**, 1778 (2013)
154. M.F. Mohd Nazeri, M.Z. Yahaya, A. Gursel, F. Cheani, M.N. Masri, A.A. Mohamad, Solder Surf. Mt. Technol. **31**, 52 (2019)
155. M.R. Harrison, J.H. Vincent, H.A.H. Steen, Solder Surf. Mt. Technol. **13**, 21 (2001)
156. X. Zhang, C. Li, Z. Gao, Y. Liu, Z. Ma, L. Yu, H. Li, Metals **6**, 175 (2016)
157. J.-C. Liu, S. Park, S. Nagao, M. Nogi, H. Koga, J.-S. Ma, G. Zhang, K. Suganuma, Corros. Sci. **92**, 263 (2015)
158. B.X. Vuong, N.S.H. Vu, T.D. Manh, M. Vaka, D.X. Du, N.D. Nam, Mater. Lett. **228**, 309 (2018)
159. K.I. Yokoyama, A. Nogami, J.I. Sakai, Corros. Sci. **86**, 142 (2014)
160. M. Wang, J. Wang, H. Feng, W. Ke, J. Mater. Sci.: Mater. Electron. **23**, 148 (2012)
161. M. Wang, J. Wang, H. Feng, W. Ke, Corros. Sci. **63**, 20 (2012)
162. M. Wang, J. Wang, W. Ke, J. Mater. Sci.: Mater. Electron. **25**, 5269 (2014)
163. R.K. Kaushik, U. Batra, J.D. Sharma, J. Alloys Compd. **745**, 446 (2018)
164. M.F.M. Nazeri, A.A. Mohamad, J. Alloys Compd. **661**, 516 (2016)
165. J.-C. Liu, G. Zhang, J.-S. Ma, K. Suganuma, J. Alloys Compd. **644**, 113 (2015)
166. J. Hu, T. Luo, A. Hu, M. Li, D. Mao, J. Electron. Mater. **40**, 1556 (2011)
167. J.C. Liu, Z.H. Wang, J.Y. Xie, J.S. Ma, Q.Y. Shi, G. Zhang, K. Suganuma, Corros. Sci. **112**, 150 (2016)
168. L.Y. Xu, Z.K. Zhang, H.Y. Jing, J. Wei, Y.D. Han, J. Mater. Sci.: Mater. Electron. **26**, 5625 (2015)

169. X. Zhou, Y. Shen, Surf. Coat. Technol. **235**, 433 (2013)
170. J. Wu, S. Xue, J. Wang, J. Wang, Y. Deng, J. Mater. Sci.: Mater. Electron. **29**, 19663 (2018)
171. Y.D. Han, L. Chen, H.Y. Jing, S.M.L. Nai, J. Wei, L.Y. Xu, J. Electron. Mater. **42**, 3559 (2013)
172. P. Collaboration, O. Adriani, G.C. Barbarino, G.A. Bazilevskaya, R. Bellotti, M. Boezio, E.A. Bogomolov, L. Bonechi, M. Bongi, V. Bonvicini, S. Bottai, A. Bruno, F. Cafagna, D. Campana, P. Carlson, M. Casolino, G. Castellini, M.P. De Pascale, G. De Rosa, D. Fedele, A.M. Galper, L. Grishantseva, P. Hofverberg, A. Leonov, S.V. Koldashov, S.Y. Krutkov, A.N. Kvashnin, V. Malvezzi, L. Marcelli, W. Menn, V.V. Mikhailov, M. Minori, E. Mocchiutti, M. Nagni, S. Orsi, G. Osteria, P. Papini, M. Pearce, P. Picozza, M. Ricci, S.B. Ricciarini, M. Simon, R. Sparvoli, P. Spillantini, Y.I. Stozhkov, E. Taddei, A. Vacchi, E. Vannuccini, G. Vasilyev, S.A. Voronov, Y.T. Yurkin, G. Zampa, N. Zampa, V.G. Zverev, Phys. Rev. Lett. **102**, 051101 (2009)
173. G.D. Badhwar, P.M. O'Neill, Adv. Space Res. **17**, 7 (1996)
174. R.L. Pease, IEEE Trans. Nucl. Sci. **50**, 539 (2003)
175. M.-T. Bao, Y. Wang, X.-J. Li, C.-M. Liu, C.-H. Yu, F. Cao, Microelectron. Reliab. **91**, 170 (2018)
176. G. Monnet, L. Vincent, L. Gélébart, J. Nucl. Mater. **514**, 128 (2019)
177. B. Wang, Z. Wang, C. Hu, Y. Zhao, Y. Zhang, W. Zhao, IEEE T. Magn. **54**, 1 (2018)
178. L. Pourzahedi, P. Zhai, J.A. Isaacs, M.J. Eckelman, J. Clean Prod. **142**, 1971 (2017)
179. J. Wang, S. Xue, Z. Lv, L. Wang, H. Liu, L. Wen, J. Mater. Sci.: Mater. Electron. **29**, 20726 (2018)

Publisher's Note Springer Nature remains neutral with regard to jurisdictional claims in published maps and institutional affiliations.